

# Weak Generative Sampler to Efficiently Sample Invariant Distribution of Stochastic Differential Equation

Zhiqiang Cai<sup>†</sup>, Yu Cao<sup>‡</sup>, Yuanfei Huang<sup>§</sup>, Xiang Zhou<sup>\*¶</sup>

**ABSTRACT.** Sampling invariant distributions from an Ito diffusion process presents a significant challenge in stochastic simulation. Traditional numerical solvers for stochastic differential equations require both a fine step size and a lengthy simulation period, resulting in both biased and correlated samples. Current deep learning-based method solves the stationary Fokker–Planck equation to determine the invariant probability density function in form of deep neural networks, but they generally do not directly address the problem of sampling from the computed density function. In this work, we introduce a framework that employs a weak generative sampler (WGS) to directly generate independent and identically distributed (iid) samples induced by a transformation map derived from the stationary Fokker–Planck equation. Our proposed loss function is based on the weak form of the Fokker–Planck equation, integrating normalizing flows to characterize the invariant distribution and facilitate sample generation from the base distribution. Our randomized test function circumvents the need for mini-max optimization in the traditional weak formulation. Distinct from conventional generative models, our method neither necessitates the computationally intensive calculation of the Jacobian determinant nor the invertibility of the transformation map. A crucial component of our framework is the adaptively chosen family of test functions in the form of Gaussian kernel functions with centres selected from the generated data samples. Experimental results on several benchmark examples demonstrate the effectiveness of our method, which offers both low computational costs and excellent capability in exploring multiple metastable states.

**Keywords:** stochastic differential equation, Fokker–Planck equation, invariant distribution sampling, deep learning for PDEs, generative model

**MSC2020:** 65N75, 65C20, 68T07

## 1. INTRODUCTION

Stochastic differential equations (SDEs) have been widely employed to model the evolution of dynamical systems under uncertainty. They arise in many disciplines such as physics, chemistry, biology, finance. For many realistic models, the system will reach a dynamical equilibrium in the long run, namely, the probability distribution of the system will reach an invariant measure. Computing and sampling this invariant distribution is a long-standing computational problem with applications across diverse disciplines: for instance, sampling from the invariant measure facilitates more efficient exploration of phase space, thereby enhancing our comprehension of rare events [5, 41, 68] and aiding in the estimation of physical quantities for certain distributions [40, 6] and studying the free energy [9], the Bayesian data assimilation [48] as well as studying structural biology matter [61].

In this work, we consider the following SDE on  $\mathbb{R}^d$ :

$$dX_t = b(X_t)dt + \sqrt{2}\sigma(X_t)dW_t, \quad (1)$$

\*CORRESPONDING AUTHOR.

<sup>†</sup>SCHOOL OF DATA SCIENCE, CITY UNIVERSITY OF HONG KONG, KOWLOON, HONG KONG SAR, ZQCAI3-C@MY.CITYU.EDU.HK

<sup>‡</sup>INSTITUTE OF NATURAL SCIENCES AND SCHOOL OF MATHEMATICAL SCIENCES, SHANGHAI JIAO TONG UNIVERSITY, SHANGHAI 200240, CHINA, YUCAO@SJTU.EDU.CN. YC IS SPONSORED BY SHANGHAI PUJIANG PROGRAM.

<sup>§</sup>SCHOOL OF DATA SCIENCE, CITY UNIVERSITY OF HONG KONG, KOWLOON, HONG KONG SAR, YHUAN26@CITYU.EDU.HK

<sup>¶</sup>SCHOOL OF DATA SCIENCE AND DEPARTMENT OF MATHEMATICS, CITY UNIVERSITY OF HONG KONG, KOWLOON, HONG KONG SAR, XIZHOU@CITYU.EDU.HK. XZ ACKNOWLEDGE THE SUPPORT FROM HONG KONG GENERAL RESEARCH FUNDS (11308121, 11318522, 11308323), AND THE NSFC/RGC JOINT RESEARCH SCHEME [RGC PROJECT No. N-CITYU102/20 AND NSFC PROJECT No. 12061160462].

where the vector-valued function  $b : \mathbb{R}^d \rightarrow \mathbb{R}^d$  is continuous, and  $\sigma : \mathbb{R}^d \rightarrow \mathbb{R}^{d \times w}$  is a matrix-valued function, and  $W_t$  is a  $w$ -dimensional standard Brownian motion.

The probability density of the SDE, denoted as  $p_t = \text{law}(X_t)$ , is known to evolve according to the Fokker–Planck equation  $\partial_t p_t = \mathcal{L}p_t$ , where the differential operator

$$\mathcal{L}p := \nabla \cdot (-bp) + \nabla^2 : (Dp), \quad (2)$$

and where  $\nabla^2 : (Dp) = \sum_{ij} \partial_{ij}(D_{ij}p)$  and the diffusion matrix  $D = \sigma\sigma^\top = (D_{ij})$  satisfies the uniform ellipticity that  $\lambda I \leq D(x) \leq \lambda^{-1}I$  for all  $x$  with a positive constant  $\lambda$ .

Estimating the invariant distribution  $p$  can be achieved by finding the zero eigenstate of the operator  $\mathcal{L}$ :

$$\mathcal{L}p = 0. \quad (3)$$

which is also known as the *stationary Fokker–Planck equation* (SFPE). Traditional techniques in numerical PDEs such as the finite difference method or finite element method [32, 16], can be utilized to solve SFPE. However, these methods encounter challenges due to the *curse of dimensionality*. Moreover, directly estimating the invariant distribution does not inherently provide a scheme for efficiently generating samples from this distribution, which is also a core task in many applications.

To overcome the dimensionality limitation and to achieve the goal of sample generation, Monte Carlo-based methods have been extensively studied in literature. A typical approach is to adopt numerical schemes [27, 10, 14, 20] to evolve the SDE for a sufficiently long time to generate the samples of the invariant distribution. There is an important class of reversible process where the invariant distribution has the known expression up to a constant: when the drift term of the SDE has the gradient form  $b = -\nabla U$  for some given potential function  $U$  and the diffusion coefficient is constant, the associated SDE is known as the overdamped Langevin dynamics [46, 4]; the invariant measure is then simply the Boltzmann distribution  $\propto \exp(-U(x)/k_B T)$  where  $k_B$  is the Boltzmann constant and  $T$  is the thermodynamic temperature. Under certain assumptions of confining potential, the density function  $p_t$  will converge to its unique equilibrium  $p$  exponentially fast as  $t$  goes to infinity [46]. This fast mixing property is an important ingredient for the efficiency of many Langevin-based sampling algorithms by adopting various numerical discretization schemes [14, 3, 22, 33, 4, 8, 51]. However, when the stochastic system with non-convex potential exhibits meta-stability, it takes an extremely large time for  $X_t$  to converge to the equilibrium under low temperature [34]. This challenge has attracted much attention, which has been addressed via e.g., parallel tempering method [63, 36], annealing-based methods [43]. As a remark, different from the Langevin-type dynamics, our approach below is broad and we study the general form of the SDE or the Fokker–Planck equation, provided that the invariant distribution exists, without acquiring prior knowledge about the specific form of the drift term  $b$ .

With the unprecedented success of deep neural networks in powerful expressiveness, many machine learning techniques have been developed in the past few years to parameterize and solve high-dimensional partial differential equations [25, 59, 2]. Notably, the *deep Ritz method* [13] is an early pioneering work in this area by exploiting the variational formulation of Poisson equations. The *physics-informed neural network* (PINN) [47] proposed to directly incorporate the structure of PDE into the loss function. For the particular problems to study in this work, deep learning like PINN is currently the backbone for many methods to tackle the solution of SFPE [62, 23, 53, 62, 67, 31]. Another important method, called *weak adversarial network* (WAN), was proposed to replace the  $L^2$  loss in PINN via a min-max problem, whose flexibility is an important feature to develop our methods below. The *weak collocation regression* [37] utilized the weak form of the Fokker–Planck equation but focused on the inverse stochastic problems. As discussed above, these deep learning-based PDE solvers cannot inherently sample the invariant distribution. For the machine-learning accelerated sampling methods, generative models play a significant role. Many of these models, such as variational autoencoders [29], generative adversarial networks [21], normalizing flows [11, 49], and score-based models [52] aim to learn a mapping that transports a base distribution to a target distribution. For instance, the samples of the target distribution could be a set of images. By sampling from the base distribution, we can readily generate samples from the target distribution using the trained mapping. A common situation for applying generative models to sampling is that the potential energy for the Boltzmann distribution is known, and normalizing flow-based methods have been used to facilitate the sampling of the target distribution

[17, 44]. To save the cost of computing Jacobian determinant for full matrix, [39, 45, 65] and [58, 55, 66] adopted the triangular building blocks for generative maps.

The collective power of deep learning methods like PINN and generative models enable us to simultaneously achieve estimating the density and sample from invariant distribution, while avoiding the curse of dimensionality. Recently, [55, 66] proposed the method called *Adaptive Deep Density Approximation* (ADDA), which is based on PINN to utilize normalizing flow to parameterize the invariant measure, and subsequently employ the PINN loss to train the normalizing flow. However, like normalizing flow and other transport-based generative models, this method requires the time-consuming computation of the Jacobian determinant. This issue is worsen in the PINN formalism due to the need to take higher-order derivatives of the differential operator  $\mathcal{L}$  in (2).

## Our contributions

In this paper, we focus on estimating the density distribution  $p$  and sampling the invariant measure of the stochastic differential equations (1). We consider the case where the drift term  $b$  and the diffusion matrix  $\sigma$  are known, and our primary goal is to sample the invariant measure of the SDE (1). It is important to note that the drift term  $b$  is *not* assumed to have a gradient form, which implies that the invariant distribution is unlikely to have a simple, closed-form expression.

To address this, we propose a novel method called the *weak generative sampler* (WGS), which samples from the invariant measure based on the weak formalism of the stationary Fokker–Planck equation. This allows the loss function to be expressed as an expectation with respect to the invariant measure. We employ normalizing flow (NF) to parameterize the transport map from the base distribution to the invariant distribution. This approach enables us to approximate the loss function using sample data points generated by the normalizing flow, without the need to compute the Jacobian determinant.

The main contributions of this work are as follows:

- **Robust and efficient method**

- (1) **Jacobi-free generator:** For our problem of invariant measure, the computation of the loss function does not involve calculating the Jacobian determinant of the normalizing flow, as no explicit expression of the density function is needed. This can generally accelerate the process by an order of magnitude.
- (2) **Randomized test function:** Our method leverages the weak formulation of SFPE but does not rely on formulated by the minimax optimization. By randomizing the test function, the algorithm becomes more robust and opens the door to adaptive training design. This not only reduces computational costs but also helps address the classic issue of mode collapse in generative models.

- **Theoretical guaranteed:** We provide a rigorous theoretical analysis to establish the bounds on the squared  $L^2$  error between the estimated density function and the true density function. Additionally, the theoretic result suggests hints of *a priori* choice of test function; see Theorems 3.1 and 3.2.

- **Numerical verification:** We conduct numerical experiments on both low and high-dimensional problems, with or without the presence of meta-stable states. We compare our WGS with the method in [54] and demonstrate that the WGS achieves comparable accuracy with a significantly lower computational cost. Furthermore, the WGS can explore all the meta-stable states in both low temperature and high temperature scenarios.

The rest of the paper is organized as follows. In Section 2, we will discuss the framework of WGS, including the network structure and, in particular, the construction of the loss function and the test functions. In Section 3, we develop the theoretical error analysis for WGS, and in Section 4, we present four numerical examples to illustrate the efficacy of WGS. Finally, we conclude the paper in Section 5.

## 2. NUMERICAL METHODS

First, we explain the weak formalism and the motivations behind our proposed method in Section 2.1. Next, in Section 2.2, we develop the weak generative sampler, covering both the

theoretical aspects and the empirical loss function used in practice. The network structure and algorithms are detailed in Sections 2.3 and 2.4, respectively.

### 2.1. Fokker–Planck equations and test functions

The invariant distribution  $p$ , with properties  $p(x) \geq 0$  and  $\int_{\mathbb{R}^d} p(x) dx = 1$ , is governed by the stationary Fokker–Planck equation (SFPE):

$$\mathcal{L}p(x) = 0, \quad \forall x \in \mathbb{R}^d.$$

Given any test function  $\varphi \in C_c^\infty(\mathbb{R}^d)$ , the SFPE then gives

$$\langle \varphi, \mathcal{L}p \rangle = 0, \quad \forall \varphi \in C_c^\infty(\mathbb{R}^d), \quad (4)$$

where  $\langle f, g \rangle := \int_{\mathbb{R}^d} f(x)g(x) dx$  is the standard  $L^2$  inner product  $L^2(\mathbb{R}^d)$ , and  $C_c^\infty(\mathbb{R}^d)$  is the set of smooth functions with compact support on  $\mathbb{R}^d$ .

To solve this SFPE, [64] proposed the form of the min-max optimization problem involving two neural network functions, one for the solution and another for the test function, by solving

$$\min_p \max_{\varphi: \|\varphi\|_2=1} |\langle \varphi, \mathcal{L}p \rangle|^2, \quad (5)$$

where  $\|\cdot\|_2$  denotes the  $L^2$ -norm in  $\mathbb{R}^d$ . Note that in theory, the optimal  $\varphi$  here is simply  $\mathcal{L}p/\|\mathcal{L}p\|_2$  and (5) essentially minimizes the  $L^2$  loss  $\|\mathcal{L}p\|_2$  as in the PINN. More generally, as [24] pointed out, if the  $L^2$  norm for the test function in (5) is replaced by  $L^r$  norm, then the loss function (5) becomes  $\|\mathcal{L}p\|_s$  with  $1/s + 1/r = 1$  by Hölder’s inequality. In the numerical method [64], the test functions  $\varphi$  is explicitly optimized within the family of neural network functions, so it can be heuristically seen as the discriminator in the traditional Generative Adversarial Network (GAN)[21]. Note that the loss function (5) still applies the operator  $\mathcal{L}$  on the solution, not its adjoint on the test function.

In this formalism, the optimal test function  $\varphi$  needs to be approximated in the form of neural network first as a subroutine in each iteration of the outer minimization problem. However, the min-max problem is generally prone to instability and solving the maximization problem typically requires substantial computational resources, which we would like to avoid. Moreover, estimating  $\mathcal{L}(p)$  still requires applying the differential operator to the density function  $p$ . If one employs a normalizing flow structure to parameterize  $p$ , calculating the Jacobian determinant—often the most computationally intensive step—becomes unavoidable.

### 2.2. Weak Generative Sampler

Our method, Weak Generative Sampler, is based on the adjoint operator of the Fokker–Planck operator  $\mathcal{L}$  and the representation of the probability by a generative flow map. Instead of considering (4) where calculation of partial derivatives of  $p$  in  $\mathcal{L}p$  is challenging, we work with the following *weak formulation* of the SFPE [15, 1]

$$\langle \mathcal{L}^* \varphi, p \rangle = 0, \quad \forall \varphi \in C_c^\infty(\mathbb{R}^d), \quad (6)$$

where

$$\mathcal{L}^* \varphi := b \cdot \nabla \varphi + D : \nabla \nabla \varphi.$$

is the infinitesimal generator of the stochastic process in (1) and  $D : \nabla \nabla \varphi = \sum_{ij} D_{ij} \partial_{ij}^2 \varphi$ . In the above equations,  $\mathcal{L}^*$  is the  $L^2$  adjoint of  $\mathcal{L}$ , i.e.,  $\langle v, \mathcal{L}u \rangle = \langle \mathcal{L}^*v, u \rangle$  for  $u, v \in C_c^2(\mathbb{R}^d)$ .

Equation (6) is a system of linear equations (with infinite dimension) for  $p$  to satisfy, each associated with a test function  $\varphi$ . In parallel to (5), one can solve the following minimax problem

$$\min_p \max_{\varphi: \|\varphi\|_2=1} |\langle \mathcal{L}^* \varphi, p \rangle|^2. \quad (7)$$

However, we solve this system using a probabilistic approach by randomizing the test function, which both circumvents the challenging mini-max optimization and facilitates the adaptivity.

More specifically, we consider the Banach space  $\Omega := C_c^\infty(\mathbb{R}^d)$  for the test function, and suppose  $\mathbb{P}$  is a non-degenerate probability distribution on this Banach space  $\Omega$  (we show in Appendix A

the existence of such probability measures), then solving (6) can be rewritten as

$$\min_p \int_{\Omega} |\langle \mathcal{L}^* \varphi, p \rangle|^2 d\mathbb{P}(\varphi).$$

It can be written more intuitively in the expectation form:

$$\min_p \mathbb{E}_{\varphi \sim \mathbb{P}} \left[ \mathbb{E}_{x \sim p} [\mathcal{L}^* \varphi(x)] \right]^2. \quad (8)$$

This family of randomized test functions is the key formalism for our proposed method and we call the objective function in (8) as the *randomized weak loss function* in contrast to (5) and (7). This formalism relaxes the worse-case error in (5) or (7) to the averaged-case error in (8) [57]. This relaxation does not affect the global minimizer since  $\mathbb{P}$  is non-degenerate, but in fact is inclined to improve training stability to certain extent.

Note that, in (8), we only need the sample data points of  $p$  (without its function expression), which facilitates the application of generative methods. Therefore, we introduce a transport map  $G_{\theta}$ , with  $\theta$  denoting the generic parameter, to map the base distribution (e.g., Gaussian distribution or uniform distribution) to the target distribution  $p$ . Then for any  $z \sim \rho$ , we can obtain the associated samples  $x = G_{\theta}(z)$ . Therefore, the minimization problem (8) is rewritten as

$$\min_{G_{\theta}} \mathbb{E}_{\varphi \sim \mathbb{P}} \left[ \mathbb{E}_{z \sim \rho} [\mathcal{L}^* \varphi(G_{\theta}(z))] \right]^2. \quad (9)$$

By the Monte Carlo method, the empirical loss function of the minimization problem (9) becomes

$$\min_{G_{\theta}} \frac{1}{N_{\varphi}} \sum_{j=1}^{N_{\varphi}} \left[ \frac{1}{N} \sum_{i=1}^N \mathcal{L}^* \varphi_j(G_{\theta}(z_i)) \right]^2, \quad (10)$$

where  $\varphi_j$  are sampled from the distribution  $\mathbb{P}(\varphi)$  and  $N_{\varphi}$  is the number of the test function  $\varphi_j$ ;  $z_i$  are sampled from the base distribution  $\rho$  and  $N$  is the number of sample points  $\{z_i\}$ . Unlike GANs, in our method, the test functions are selected through sampling rather than maximization. We shall show the principled guidance of adaptively selecting these test functions in the data-driven approach based on the current  $G_{\theta}$ . We name this method the *Weak Generative Sampler* (WGS).

In principle, any random function in  $\Omega = C_c^{\infty}$  with non-degenerate probability on a dense (countable) subset of  $\Omega$  can guarantee the validity of our method. One can choose the test function in the space  $\sum_k c_k \phi_k$  spanned by the orthonormal basis functions  $\{\phi_k\}$  in  $\Omega$ , such as the Hermite polynomials [7], or eigen-functions of  $\mathcal{L}$ . Then the probability  $\mathbb{P}$  supported on the unit ball  $\{\|\vec{c}\| = 1 : \vec{c} = (c_k)\}$  is sufficient. Using some reproducing kernel Hilbert space as a dense subset of  $\Omega$  with kernel mean embedding of distribution is also feasible [42].

However, if the choice of these test functions are pre-determined and static, the number of test functions used in computation will be huge and the training efficiency will not be satisfactory at all, since it is unable to provide the informative guidance during the training of the map  $G_{\theta}$ . We propose the following adaptive idea base on the data-informed test function. Firstly, our numerical scheme here uses the family of Gaussian kernel functions given by:

$$\varphi_j(x) = \exp\left(-\frac{1}{2\kappa^2} \|x - \zeta_j\|_2^2\right), \quad j \in \{1, 2, \dots, N_{\varphi}\}, \quad (11)$$

where  $\zeta_j$  represents the centers and the hyper-parameter  $\kappa$  is the scale length determining the width of the kernel. The Gaussian kernel gives the infinitely differentiable functions  $\varphi$  that decay at infinity. Then the distribution  $\mathbb{P}$  on the space of the test function is determined by the distribution of the  $N_{\varphi}$  center points  $\{\zeta_j\}_{j=1}^{N_{\varphi}}$ .  $\kappa$  is a hyper-parameter in the training which can be fixed or adaptively chosen. We consider two extreme cases of  $\kappa$ . If  $\kappa \rightarrow \infty$ , then  $\varphi_j$  become constant functions, in the null space of  $\mathcal{L}^*$ , and therefore the weak loss function (8) is zero. If  $\kappa \rightarrow 0$ , then  $\langle \mathcal{L}^* \varphi_j, p \rangle = \langle \varphi_j, \mathcal{L}p \rangle \rightarrow \mathcal{L}p(\zeta_j)$  and the loss (8) becomes the least-square loss used in the PINN:  $\mathbb{E}_{\zeta} |\mathcal{L}p(\zeta)|^2$ . Many acceleration techniques for training the PINN are based on the intuitive choice of the distribution for the training sample  $\zeta$  [24, 18, 66, 55, 38]. Our method uses a finite value of  $\kappa$  so that the test function  $\varphi_j$  reflects the information in a neighbor of size  $\kappa$  around, but not strictly limited to, a point  $\zeta_j$ ; the rational choice of  $\kappa$  will be discussed and validated in later text.

Secondly, our adaptive choice of the centers  $\zeta$  in the test functions  $\varphi$  shares the same distribution as the generated data, which approximates the true solution  $p$ . Specifically,  $N_\varphi$  is set to be less than  $N$  and the collection of  $\{\zeta_j\}_{j=1}^{N_\varphi}$  is uniformly selected without replacement from the total number of particles  $N$  data points  $\{x_i = G_\theta(z_i)\}$  used in training the loss (10). To introduce variability for better exploration, we also add an independent small Gaussian noise to these selected data points, giving

$$\zeta_j = x_{(j)} + \gamma \mathcal{N}(0, \mathbf{I}_d)$$

with a small parameter  $\gamma > 0$ , where  $x_{(j)}$ ,  $1 \leq j \leq N_\varphi$ , are sampled without replacement from the collection  $\{x_i, 1 \leq i \leq N\}$ . The size  $N_\varphi$  is usually only a small fraction of the total particle numbers  $N$ . In summary, the choice of the center points for the test function is adaptive and informative since it is based on the samples generated from the map  $G_\theta$  during the training. We illustrate our scheme in the Figure 1.

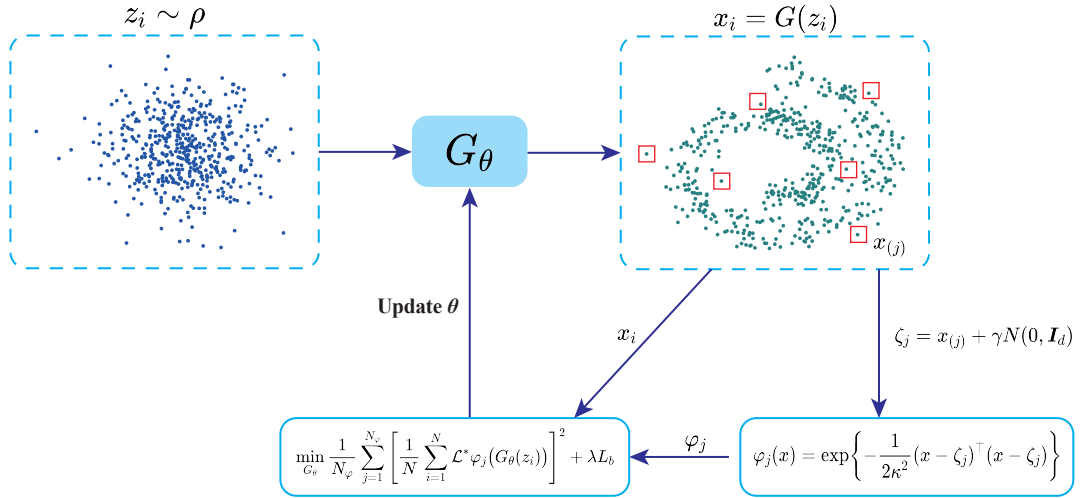


FIGURE 1. The framework of WGS. In WGS, data points  $\{z_i\}_{i=1}^N$  are sampled from the base distribution  $\rho$  and transformed to  $\{x_i\}_{i=1}^N$  via the transport map  $G_\theta$ . Then,  $\{x_{(j)}\}_{j=1}^{N_\varphi}$  are selected uniformly from  $\{x_i\}_{i=1}^N$ , and Gaussian noise is added to obtain  $\{\zeta_j\}_{j=1}^{N_\varphi}$ . The loss function is derived from data points  $\{x_i\}_{i=1}^N$  and test functions  $\{\varphi_j\}_{j=1}^{N_\varphi}$ . The transport map  $G_\theta$  is updated through gradient descent. The term  $\lambda L_b$  is a penalty term from the boundary; see (12) for details.

### 2.3. Network structure of $G_\theta$

The transport map  $G_\theta$  is a differentiable transformation from the base distribution to the target distribution. By the change-of-variable formula [30], the probability density function associated with an invertible map  $G_\theta$  is

$$p_\theta(x) = \rho(G_\theta^{-1}(x)) |\det \nabla G_\theta^{-1}(x)|.$$

So the computation of the density function  $p_\theta$  itself involves calculating the determinant of the Jacobians and does not allow the degeneracy of the Jacobian matrix. However, for generative purpose only as in our method, neither the Jacobian determinant nor invertibility is necessary.

Normalizing flows [49, 50] are a family of invertible neural networks and provide a way to construct the transport map  $G$  as the composition of a sequence of functions  $\{g_{\theta_i}\}_{i=1}^L$ :

$$G_\theta = g_{\theta_L} \circ g_{\theta_{L-1}} \circ \cdots \circ g_{\theta_1},$$

parameterized by  $\theta = (\theta_1, \theta_2, \dots, \theta_L)$  and  $x = G_\theta(z)$ . These functions serve to gradually transform the sample data point  $z$  from the base distribution  $\rho$  into the sample data point  $x$  following the target distribution  $p$ . Explicitly, we have

$$x^{(i)} = g_{\theta_i}(x^{(i-1)}), \quad i \in \{1, 2, \dots, L\},$$

where  $x^{(0)} = z$  and  $x^{(L)} = x$ . One popular example for constructing the parameterized function  $g_{\theta_i}$  is via the triangular form and shuffled with each other by random coordinates. In this paper, we use a simple yet expressive affine coupling layer in the RealNVP [11, 56]. In RealNVP, the affine coupling layer  $g_{\theta_i}$  is defined as

$$x^{(i)} = g_{\theta_i} \left( x_1^{(i-1)}, x_2^{(i-1)} \right) = \left( h_i \left( x_1^{(i-1)}; \Theta_i \left( x_2^{(i-1)} \right) \right), x_2^{(i-1)} \right), \quad i \in \{1, 2, \dots, L\},$$

where  $(x_1^{(i-1)}, x_2^{(i-1)}) \in \mathbb{R}^a \times \mathbb{R}^{d-a}$  is the partition<sup>1</sup> of  $x^{(i-1)}$ , and  $\Theta_i : \mathbb{R}^{d-a} \mapsto \mathbb{R}^a$  is parameterized by  $\theta_i = (\theta_i^1, \theta_i^2)$ . Here,  $h_i : \mathbb{R}^d \mapsto \mathbb{R}^d$  is the coupling function that is defined as

$$h_i \left( x_1^{(i-1)}; \Theta_i \left( x_2^{(i-1)} \right) \right) = \left( x_1^{(i-1)} - t_{\theta_i^1} \left( x_2^{(i-1)} \right) \right) \odot \exp \left( -s_{\theta_i^2} \left( x_2^{(i-1)} \right) \right).$$

Here,  $t_{\theta_i^1} : \mathbb{R}^{d-a} \mapsto \mathbb{R}^a$  and  $s_{\theta_i^2} : \mathbb{R}^{d-a} \mapsto \mathbb{R}^a$  are the translation and scaling functions, respectively. These functions are parameterized by neural networks with parameters  $\theta_i^1$  and  $\theta_i^2$ , respectively.

Since the affine coupling layer  $g_{\theta_i}$  only updates  $x_1^{(i-1)}$ , we can update  $x_2^{(i)}$  in the subsequent affine coupling layer  $g_{\theta_{i+1}}$ . This ensures that all components in  $z$  are updated after transformation by the transport map  $G_{\theta}$ . This allows for more flexibility in the partition of  $x^{(i)}$  and the arrangement of the affine coupling layers. Other popular coupling layers include splines and the mixtures of cumulative distribution functions, which have been shown to be more expressive than the affine coupling function [12, 26, 28, 54]. In principle, any network structure for the map can work effectively for our weak generative sampler. The details about the improvement of training performance and expressive power are beyond the scope of our work here.

#### 2.4. Training algorithm

---

##### Algorithm 1: Training Algorithm of WGS

---

**Input** : Initial flow map  $G_{\theta}$ , the base distribution  $\rho$ ; the hyper-parameters  $\gamma > 0$ ,  $\kappa > 0$ ,  $\lambda > 0$ ,  $r > 0$ ,  $c > 0$ .

1 **for**  $n = 1 : N_I$  **do**

2     Sample  $\{z_i\}_{i=1}^N$  from  $\rho$ ;

3     Obtain  $\{x_i\}_{i=1}^N$  by  $x_i = G_{\theta}(z_i)$ ;

4     Randomly choose  $N_{\varphi}$  numbers from  $1 : N$  as index  $ind$ ;

5     Obtain  $\{x_{(j)}\}_{j=1}^{N_{\varphi}}$  by  $x_{(j)} = x_{ind(j)} + \gamma \mathcal{N}(0, \mathbf{I}_d)$ ;

   //  $\mathcal{N}(0, \mathbf{I}_d)$  denotes the standard  $d$ -dimensional normal random variables;

6     Construct the test function  $\varphi_j$  by Gaussian kernel as

$$\varphi_j(x) = \exp \left\{ -\frac{1}{2\kappa^2} (x - x_{(j)})^{\top} (x - x_{(j)}) \right\},$$

   // The parameter  $\kappa$  denotes the standard deviation in each dimension;

7     Compute the Loss function (12);

8     Update the parameters  $\theta$  using the Adam optimizer with a learning rate  $\eta$ ;

9 **end**

**Output:** The optimal transport map  $G_{\theta}$

---

We now summarize the training algorithm of our method. Since we are solving the SFPE on the whole  $\mathbb{R}^d$  space, it is important in practice to restrict the map from pushing all points to infinitely far away, since any constant function satisfies  $\mathcal{L}p = 0$ . We propose to constrain the range of the map within a ball with a large radius of  $r$  by adding a penalty term  $L_b$  to the loss (10):

$$L(G_{\theta}) = \frac{1}{N_{\varphi}} \sum_{j=1}^{N_{\varphi}} \left[ \frac{1}{N} \sum_{i=1}^N \mathcal{L}^* \varphi_j(G_{\theta}(z_i)) \right]^2 + \lambda L_b, \quad (12)$$

<sup>1</sup>This partition of  $x^{(i)}$  can be randomized in practice.

where

$$L_b = \frac{1}{N} \sum_{i=1}^N \text{Sigmoid}\left(c(\|G_\theta(z_i) - x_0\|_2^2 - r^2)\right)$$

and the positive numbers  $\lambda, r$ , and  $c$  are hyper-parameters and  $\text{Sigmoid}(x) = 1/(1 + \exp(-x))$ . More specifically, we apply a large penalty to samples outside of the ball  $B_r(x_0)$ ; the parameters  $c$  and  $\lambda$  essentially control the extent to which we want the push-forward probability measure  $G_\theta\#\rho$  to be confined within the region  $B_r(x_0)$ . Algorithm 1 shows the whole algorithm of our method.

### 3. $L^2$ ERROR ESTIMATE OF WGS

As mentioned earlier, our weak generative sampler addresses the optimization problem (8) by minimizing the following loss function derived from the weak form of the stationary Fokker–Planck equation (3),

$$\int_{\Omega} \left| \int_{\mathbb{R}^d} \mathcal{L}^* \varphi(x) p(x) dx \right|^2 d\mathbb{P}(\varphi), \quad (13)$$

which can be written in the expectation form

$$\mathbb{E}_{\varphi \sim \mathbb{P}} |\mathbb{E}_{x \sim p} \mathcal{L}^* \varphi(x)|^2.$$

Here  $\mathbb{P}$  is a non-degenerate probability on the space of test functions  $\varphi$ . The basic requirement for  $\mathbb{P}$  is that the zero loss value of (13) can imply Equation (6) for the minimizer  $p$ .

To highlight the core idea of our proof, we first focus on the Fokker–Planck equation with periodic boundary conditions on a torus, as detailed in Section 3.1. This setting helps us avoid the intricate technical problems associated with compactness that usually arise from boundary conditions at infinity. Subsequently, the extension to the whole space  $\mathbb{R}^d$  is covered in Section 3.2.

#### 3.1. Stationary Fokker–Planck equations in periodic domain

For given positive constants  $\{R_i\}_{i=1}^d$ , let  $U := \prod_{i=1}^d (0, R_i) \subset \mathbb{R}^d$ . In the Fokker–Planck operator  $\mathcal{L}$  defined in (2), the drift term  $b$  and diffusion matrix  $\sigma$  are assumed to be  $U$ -periodic, i.e., they admit period  $R_i$  in the  $i$ -th direction,  $i = 1, \dots, d$ . We assume that  $b \in C_{per}^1(U)$  and  $D \in C_{per}^2(U)$ , and assume that  $p$  is the unique classic nontrivial solution to the stationary Fokker–Planck equation on the torus  $U$ ,

$$\mathcal{L}p = 0, \quad \text{in } U, \quad (14)$$

and  $p$  satisfies the periodic boundary condition and normalization condition  $\int_U p(x) dx = 1$ . The solution  $p$  can also be interpreted as a weak function in the periodic Sobolev space  $H_{per}^1(U)$ , the Sobolev space consisting of  $U$ -periodic functions whose first weak derivatives exist and  $L^2$  integrable on  $U$ , so  $p$  satisfies

$$\int_U \mathcal{L}^* \varphi(x) p(x) dx = 0, \quad \forall \varphi \in \Omega_0 := C_0^\infty(U). \quad (15)$$

In the numerical computation of minimizing (8), the probability density function belongs to a family parametrized by a generic parameter  $\theta$  in a specific set  $\Theta$ :  $\{p_\theta\}_{\theta \in \Theta}$ . This following assumption is trivially fulfilled in our setting here.

**Assumption 1.** *We make the following assumptions about the family of the density function  $p_\theta$  that for all  $\theta \in \Theta$*

$$0 \leq p_\theta(x) \leq M, \quad \forall x \in U; \quad \int_U p_\theta(x) dx = 1.$$

where  $M$  is a constant.

Our result about the  $L^2$  error and the loss (13) needs the following assumption of the probability  $\mathbb{P}$  on the space of the test function  $\Omega_0 = C_0^\infty(U)$ . The rigorous statement about existence and construction of such probability measures  $\mathbb{P}$  is shown in Appendix A.

**Assumption 2.** (1) *For any positive number  $r$  and  $f \in L^2(U)$ , it holds that*

$$\mathbb{P}(\bar{B}_{L^2(U)}(f, r) \cap C_0^\infty(U)) > 0,$$

where  $\bar{B}_{L^2(U)}(f, r) = \{g \in L^2(U) : \|f - g\|_{L^2(U)} \leq r\}$  is the closed ball centered at  $f$  with  $r$  radius in  $L^2(U)$ .

(2) For any positive number  $r$  and  $f \in H^2(U)$ , it holds that

$$\mathbb{P}(\bar{B}_{H^2(U)}(f, r) \cap C_0^\infty(U)) > 0,$$

where  $\bar{B}_{H^2(U)}(f, r) = \{g \in H^2(U) : \|f - g\|_{H^2(U)} \leq r\}$  is the closed ball centered at  $f$  with  $r$  radius in  $H^2(U)$ .

Our theorem below asserts that with a properly chosen test function, the weak loss closely approximates the mean square loss relative to the true solution.

**Theorem 3.1.** *Let  $U \subset \mathbb{R}^d$  be a torus. Let  $p \in C_{per}^2(U)$  be the classical solution of the stationary Fokker–Planck equation (14) on the torus  $U$ . Suppose that  $p_\theta \in C_{per}^2(U)$  for every  $\theta \in \Theta$ , and Assumption 1 holds. For any  $\theta \in \Theta$ , define  $\varphi_\theta$  as the solution to the Dirichlet boundary value problem*

$$\begin{cases} \mathcal{L}^* \varphi_\theta = p_\theta - p, & \text{in } U, \\ \varphi_\theta = 0, & \text{on } \partial U. \end{cases} \quad (16)$$

Let  $\mathbb{P}_{\theta, r}(\cdot)$ ,  $\mathbb{P}'_{\theta, r}(\cdot)$  denote the conditional distributions  $\mathbb{P}(\cdot | \bar{B}_{L^2(U)}(\varphi_\theta, r))$  and  $\mathbb{P}(\cdot | \bar{B}_{H^2(U)}(\varphi_\theta, r))$  respectively.

(a) If Assumption 2-(1) holds, then for any  $r > 0$ ,

$$\mathbb{E}_{\varphi \sim \mathbb{P}_{\theta, r}} |\mathbb{E}_{x \sim p_\theta} \mathcal{L}^* \varphi(x)| - r \|\mathcal{L} p_\theta\|_{L^2(U)} \leq \|p_\theta - p\|_{L^2(U)}^2 \leq \mathbb{E}_{\varphi \sim \mathbb{P}_{\theta, r}} |\mathbb{E}_{x \sim p_\theta} \mathcal{L}^* \varphi(x)| + r \|\mathcal{L} p_\theta\|_{L^2(U)}, \quad (17)$$

(b) If Assumption 2-(2) holds, then for any  $r > 0$ ,

$$\mathbb{E}_{\varphi \sim \mathbb{P}'_{\theta, r}} |\mathbb{E}_{x \sim p_\theta} \mathcal{L}^* \varphi(x)| - rC \leq \|p_\theta - p\|_{L^2(U)}^2 \leq \mathbb{E}_{\varphi \sim \mathbb{P}'_{\theta, r}} |\mathbb{E}_{x \sim p_\theta} \mathcal{L}^* \varphi(x)| + rC, \quad (18)$$

where

$$C = M \left( d \max_i \|b_i\|_U + d^2 \max_{i,j} \|D_{ij}\|_U \right). \quad (19)$$

**Remark 1.** Note that a measurable functional  $F$ , the conditional expectation  $\mathbb{E}_{\varphi \sim \mathbb{P}_{\theta, r}} F(\varphi) = \mathbb{E}_{\varphi \sim \mathbb{P}} [F(\varphi) \mathbf{1}_{\bar{B}(\varphi_\theta, r)}(\varphi)] / \mathbb{P}(\bar{B}(\varphi_\theta, r)) \leq \mathbb{E}_{\varphi \sim \mathbb{P}} [F(\varphi)] / \mathbb{P}(\bar{B}(\varphi_\theta, r))$ . So, the above upper bounds can be replaced by  $\mathbb{E}_{\varphi \sim \mathbb{P}} |\mathbb{E}_{x \sim p_\theta} \mathcal{L}^* \varphi(x)| / \mathbb{P}(\bar{B}(\varphi_\theta, r))$ . In addition, according to Jensen's inequality, the quadratic form of our loss function (13) is the upper bound of the term  $\mathbb{E}_{\varphi \sim \mathbb{P}} |\mathbb{E}_{x \sim p_\theta} \mathcal{L}^* \varphi(x)|$ :  $\left( \int_{\Omega_0} |\int_U \mathcal{L}^* \varphi(x) p(x) dx| d\mathbb{P}(\varphi) \right)^2 \leq \int_{\Omega_0} |\int_U \mathcal{L}^* \varphi(x) p(x) dx|^2 d\mathbb{P}(\varphi)$ .

**Remark 2.** In the limit of  $r \rightarrow 0$ ,  $\mathbb{E}_{\varphi \sim \mathbb{P}_{\theta, r}} |\mathbb{E}_{x \sim p_\theta} \mathcal{L}^* \varphi(x)|$  tends to  $|\mathbb{E}_{x \sim p_\theta} \mathcal{L}^* \varphi_\theta(x)|$  which exactly recovers the squared  $L^2$  error  $\|p - p_\theta\|_{L^2(U)}^2$ . In general, for a finite  $r$ , our results heuristically suggest that it is desirable for the probability  $\mathbb{P}$  of sampling the test function to adaptively primarily concentrate within a small ball around  $\varphi_\theta$ . Note that  $\varphi_\theta$  can be regarded as an a priori estimation of the error between  $p_\theta$  and the solution  $p$ .

*Proof.* Since  $p_\theta$  and the true solution  $p$  both in  $C_{per}^2(U)$ , the Dirichlet problem (16) has a unique  $C_{per}^{2,1}(U)$  solution  $\varphi_\theta$ . Then we can write the squared  $L^2$  error between  $p_\theta$  and  $p$  in terms of  $\varphi_\theta$ :

$$\int_U |p_\theta(x) - p(x)|^2 dx = \int_U \mathcal{L}^* \varphi_\theta(x) (p_\theta(x) - p(x)) dx = \int_U \mathcal{L}^* \varphi_\theta(x) p_\theta(x) dx, \quad (20)$$

by using the fact that  $p$  is the true solution satisfying the periodic boundary condition and  $\varphi_\theta$  vanishes on  $\partial U$ .

Let  $r$  be a positive constant. Use a concise notation  $\Omega_{\theta, r} := \{\varphi \in C_0^\infty(U) : \|\varphi - \varphi_\theta\|_{L^2(U)} \leq r\} \subset \Omega_0$  to represent the  $L^2$ -ball. By Assumption 2 we know that the conditional distribution  $\mathbb{P}_{\theta, r}(\cdot) = 1$  is well-defined and  $\mathbb{P}_{\theta, r}(\Omega_{\theta, r}) = 1$ . We now obtain the bound for the squared  $L^2$  error

$\|p_\theta - p\|_{L^2(U)}^2$  below. Note that,

$$\begin{aligned}
& \int_{\Omega_0} \left| \int_U \mathcal{L}^* \varphi(x) p_\theta(x) dx \right| d\mathbb{P}_{\theta,r}(\varphi) = \int_{\Omega_{\theta,r}} \left| \int_U (\varphi(x) - \varphi_\theta(x) + \varphi_\theta(x)) \mathcal{L} p_\theta(x) dx \right| d\mathbb{P}_{\theta,r}(\varphi) \\
& \geq \int_{\Omega_{\theta,r}} \left| \int_U \varphi_\theta(x) \mathcal{L} p_\theta(x) dx \right| d\mathbb{P}_{\theta,r}(\varphi) - \int_{\Omega_{\theta,r}} \left( \int_U |\varphi(x) - \varphi_\theta(x)|^2 dx \right)^{1/2} \left( \int_U |\mathcal{L} p_\theta(x)|^2 dx \right)^{1/2} d\mathbb{P}_{\theta,r}(\varphi) \\
& \geq \left| \int_U \varphi_\theta(x) \mathcal{L} p_\theta(x) dx \right| \mathbb{P}_{\theta,r}(\Omega_{\theta,r}) - r \|\mathcal{L} p_\theta\|_{L^2} \mathbb{P}_{\theta,r}(\Omega_{\theta,r}), \\
& = \int_U |p_\theta(x) - p(x)|^2 dx - r \|\mathcal{L} p_\theta\|_{L^2(U)}.
\end{aligned} \tag{21}$$

This implies the inequality “ $\geq$ ” for (17). We can prove “ $\leq$ ” part in a similar way by revising the second line in the above derivation (21) by using  $|\varphi(x) - \varphi_\theta(x) + \varphi_\theta(x)| \leq |\varphi_\theta(x)| + |\varphi(x) - \varphi_\theta(x)|$ .

The proof for the second statement (18) follows a similar approach to the one above, albeit with some minor differences. Define the  $H^2$ -ball  $\Omega'_{\theta,r} := \{\varphi \in C_0^\infty(U) : \|\varphi - \varphi_\theta\|_{H^2(U)} \leq r\}$ . Then we have

$$\begin{aligned}
& \mathbb{E}_{\varphi \sim \mathbb{P}'_{\theta,r}} |\mathbb{E}_{x \sim p_\theta} \mathcal{L}^* \varphi(x)| = \int_{\Omega'_{\theta,r}} \left| \int_U \mathcal{L}^* (\varphi(x) - \varphi_\theta(x) + \varphi_\theta(x)) p_\theta(x) dx \right| d\mathbb{P}'_{\theta,r}(\varphi) \\
& \geq \left| \int_U \mathcal{L}^* \varphi_\theta(x) p_\theta(x) dx \right| \mathbb{P}'_{\theta,r}(\Omega'_{\theta,r}) - \int_{\Omega'_{\theta,r}} \int_U \left| \sum_{i=1}^d b_i(x) (\partial_{x_i} \varphi(x) - \partial_{x_i} \varphi_\theta(x)) \right. \\
& \quad \left. + \sum_{i,j=1}^d D_{ij}(x) (\partial_{x_j x_i}^2 \varphi(x) - \partial_{x_j x_i}^2 \varphi_\theta(x)) \right| p_\theta(x) dx d\mathbb{P}'_{\theta,r}(\varphi) \\
& \geq \left| \int_U \mathcal{L}^* \varphi_\theta(x) p_\theta(x) dx \right| \mathbb{P}'_{\theta,r}(\Omega_{\theta,r}) - \int_{\Omega'_{\theta,r}} \|\varphi - \varphi_\theta\|_{H^2(U)} \\
& \quad \times \left[ \sum_{i=1}^d \left( \int_U |b_i(x) p_\theta(x)|^2 dx \right)^{1/2} + \sum_{i,j=1}^d \left( \int_U |D_{ij}(x) p_\theta(x)|^2 dx \right)^{1/2} \right] d\mathbb{P}'_{\theta,r} \\
& \geq \int_U |p_\theta(x) - p(x)|^2 dx - rC,
\end{aligned} \tag{22}$$

where  $C$  is defined in (19). The proof for the converse inequality side is the same as that for the first statement.  $\square$

### 3.2. Stationary Fokker–Planck equations in $\mathbb{R}^d$

Under mild assumption<sup>2</sup> of the drift  $b(x)$  and the uniform elliptic diffusion  $\sigma(x)$ , the SDE (1) is ergodic and the Fokker–Planck equation has a unique invariant probability density function on the entire space  $\mathbb{R}^d$  which decays at infinity. The similar results to Theorem 3.1 can be derived.

For simplicity, we assume the drift term and the functions in the diffusion matrix are bounded.

**Assumption 3.** *Suppose  $\|b_i\|_\infty < \infty$  and  $\|\sigma_{ij}\|_\infty < \infty$  for  $i, j \in \{1, \dots, d\}$ .*

We list the assumptions concerning the family of probability density functions  $\{p_\theta\}_{\theta \in \Theta}$  and the probability measure  $\mathbb{P}$  on the test function space  $\Omega = C_c^\infty(\mathbb{R}^d)$ .

#### Assumption 4.

(1) *There exists a positive constant  $M$  such that for every  $\theta \in \Theta$ ,*

$$0 \leq p_\theta(x) \leq M, \quad \forall x \in \mathbb{R}^d, \quad \int_{\mathbb{R}^d} p_\theta(x) dx = 1.$$

<sup>2</sup>For example, there is a domain  $A \subset \mathbb{R}^d$  so that all flow of the vector field  $b$  are attracted to  $D$  and  $b(x) \cdot n(x) < 0$  for all  $x \in \partial A$ , where  $n(x)$  is the exterior normal of the boundary of  $A$ .

- (2) The family functions  $\{p_\theta\}_{\theta \in \Theta}$  and  $p$  are uniformly tight, i.e., for every  $\varepsilon > 0$  there exists a compact subset  $U_\varepsilon \subset \mathbb{R}^d$  such that for all  $\theta \in \Theta$  and  $p$

$$\int_{U_\varepsilon^c} p_\theta(x) dx < \varepsilon, \quad \int_{U_\varepsilon^c} p(x) dx < \varepsilon.$$

Without loss generality, for such given  $\varepsilon$  we assume there exists a positive constant  $r_\varepsilon$  such that  $U_\varepsilon = \bar{B}_{r_\varepsilon}$ , the closed ball centered at 0 with radius  $r_\varepsilon$  in  $\mathbb{R}^d$ . In addition, we assume

$$0 \leq p_\theta(x), p(x) < 1, \quad \forall x \in B_{r_\varepsilon}^c, \theta \in \Theta.$$

- (3) The probability measure  $\mathbb{P}$  satisfies that for any given positive number  $r > 0$ , it holds that

$$\mathbb{P}(\bar{B}_{L^2(\mathbb{R}^d)}(f, r) \cap C_c^\infty(\mathbb{R}^d)) > 0,$$

where  $\bar{B}_{L^2(\mathbb{R}^d)}(f, r) = \{g \in L^2(\mathbb{R}^d) : \|f - g\|_{L^2(\mathbb{R}^d)} \leq r\}$  is the closed ball centered at  $f$  and with radius  $r$  in  $L^2(\mathbb{R}^d)$ .

- (4) The probability measure  $\mathbb{P}$  satisfies that for any given positive number  $r > 0$ , it holds that

$$\mathbb{P}(\bar{B}_{H^2(\mathbb{R}^d)}(f, r) \cap C_c^\infty(\mathbb{R}^d)) > 0,$$

where  $\bar{B}_{H^2(\mathbb{R}^d)}(f, r) = \{g \in H^2(\mathbb{R}^d) : \|f - g\|_{H^2(\mathbb{R}^d)} \leq r\}$  is the closed ball centered at  $f$  and with radius  $r$  in  $H^2(\mathbb{R}^d)$ .

**Theorem 3.2.** Let  $p \in C^2(\mathbb{R}^d)$  be the classical solution of the stationary Fokker–Planck equation (3). Suppose that  $p_\theta \in C^2(\mathbb{R}^d)$  for every  $\theta \in \Theta$ , Assumption 3 and 4-(1)-(2) hold. For any  $\varepsilon > 0$ , let  $\varphi_{\theta, \varepsilon}$  be the solution to the boundary value Dirichlet problem on the ball  $B_{r_\varepsilon}$ ,

$$\begin{cases} \mathcal{L}^* \varphi_{\theta, \varepsilon} = p_\theta - p, & \text{in } B_{r_\varepsilon}, \\ \varphi_{\theta, \varepsilon} = 0, & \text{on } \partial B_{r_\varepsilon}, \end{cases} \quad (23)$$

and extend the definition  $\varphi_{\theta, \varepsilon} = 0$  in  $B_{r_\varepsilon}^c$ . Let  $\mathbb{P}_{\theta, r, \varepsilon}(\cdot)$ ,  $\mathbb{P}'_{\theta, r, \varepsilon}(\cdot)$  be the conditional distributions  $\mathbb{P}(\cdot | \bar{B}_{L^2(\mathbb{R}^d)}(\varphi_{\theta, \varepsilon}, r))$  and  $\mathbb{P}(\cdot | \bar{B}_{H^2(\mathbb{R}^d)}(\varphi_{\theta, \varepsilon}, r))$  respectively.

- (a) If Assumption 4-(3) holds, then for any  $r > 0$ ,

$$\mathbb{E}_{\varphi \sim \mathbb{P}_{\theta, r, \varepsilon}} |\mathbb{E}_{x \sim p_\theta} \mathcal{L}^* \varphi(x)| - r \|\mathcal{L} p_\theta\|_2 \leq \|p_\theta - p\|_2^2 \leq \mathbb{E}_{\varphi \sim \mathbb{P}_{\theta, r, \varepsilon}} |\mathbb{E}_{x \sim p_\theta} \mathcal{L}^* \varphi(x)| + r \|\mathcal{L} p_\theta\|_2 + \varepsilon. \quad (24)$$

- (b) If Assumption 4-(4) holds, then for any  $r > 0$ ,

$$\mathbb{E}_{\varphi \sim \mathbb{P}'_{\theta, r}} |\mathbb{E}_{x \sim p_\theta} \mathcal{L}^* \varphi(x)| - rC \leq \|p_\theta - p\|_2^2 \leq \mathbb{E}_{\varphi \sim \mathbb{P}'_{\theta, r}} |\mathbb{E}_{x \sim p_\theta} \mathcal{L}^* \varphi(x)| + rC + \varepsilon, \quad (25)$$

where

$$C = M \left[ d \max_i \|b_i\|_\infty + d^2 \max_{i,j} \|D_{ij}\|_\infty \right]. \quad (26)$$

*Proof.* According to Assumption 4-(2), we observe that the  $L^2$  error primarily concentrates within the bounded domain  $B_{r_\varepsilon}$ ,

$$\begin{aligned} \int_{B_{r_\varepsilon}} |p_\theta(x) - p(x)|^2 dx &\leq \int_{\mathbb{R}^d} |p_\theta(x) - p(x)|^2 dx \\ &= \int_{B_{r_\varepsilon}} |p_\theta(x) - p(x)|^2 dx + \int_{B_{r_\varepsilon}^c} |p_\theta(x) - p(x)|^2 dx \\ &\leq \int_{B_{r_\varepsilon}} |p_\theta(x) - p(x)|^2 dx + \varepsilon. \end{aligned} \quad (27)$$

And  $p_\theta - p$  is at least  $C^1$  in  $\mathbb{R}^d$ , making the Dirichlet problem (23) have a unique  $C^{2,1}(\bar{B}_{r_\varepsilon})$  solution (see [19, Theorem 6.8 & Corollary 6.9]). Since  $\varphi_{\theta, \varepsilon}$  may not be in  $C^2(\mathbb{R}^d)$ , we consider its  $\delta$ -mollification

$$\widehat{\varphi}_{\theta, \varepsilon, \delta}(x) := \int_{\mathbb{R}^d} \eta_\delta(x - y) \widehat{\varphi}_{\theta, \varepsilon}(y) dy = \int_{B_\delta} \eta_\delta(y) \widehat{\varphi}_{\theta, \varepsilon}(x - y) dy,$$

where  $\eta_\delta = \frac{1}{\delta^d} \eta\left(\frac{x}{\delta}\right)$ , and  $\eta$  is the standard mollifier

$$\eta(x) = \begin{cases} K_0 \exp\left(\frac{1}{|x|^2-1}\right), & \text{if } |x| < 1, \\ 0, & \text{if } |x| \geq 1, \end{cases}$$

and  $K_0 > 0$  is a constant selected such that  $\int_{\mathbb{R}^d} \eta dx = 1$ . It is easy to see [15, Appendix C4 & Section 5.3.1 Theorem 1] that  $\widehat{\varphi}_{\theta,\varepsilon,\delta} \in C_c^\infty(\mathbb{R}^d)$  and

$$\widehat{\varphi}_{\theta,\varepsilon,\delta} \rightarrow \varphi_{\theta,\varepsilon}, \quad \text{in } H_{\text{loc}}^2(\mathbb{R}^d), \quad \text{as } \delta \rightarrow 0.$$

Now we can estimate the squared  $L^2$  error in terms of the special test function  $\widehat{\varphi}_{\theta,\varepsilon,\delta} \in C_c^\infty(\mathbb{R}^d)$  as follows by noting  $\int_{\mathbb{R}^d} \mathcal{L}^* \widehat{\varphi}_{\theta,\varepsilon,\delta}(x) p(x) dx = 0$  for the true solution  $p$  and  $\varphi_{\theta,\varepsilon}(x) = \widehat{\varphi}_{\theta,\varepsilon,\delta}(x) = 0$  outside of  $B_{1+r_\varepsilon}$ :

$$\begin{aligned} & \int_{B_{r_\varepsilon}} |p_\theta(x) - p(x)|^2 dx = \int_{\mathbb{R}^d} \mathcal{L}^* \varphi_{\theta,\varepsilon}(x) (p_\theta(x) - p(x)) dx \\ &= \int_{\mathbb{R}^d} \mathcal{L}^* \widehat{\varphi}_{\theta,\varepsilon,\delta}(x) p_\theta(x) dx + \int_{B_{r_\varepsilon+1}} \mathcal{L}^* (\varphi_{\theta,\varepsilon}(x) - \widehat{\varphi}_{\theta,\varepsilon,\delta}(x)) (p_\theta(x) - p(x)) dx \\ &=: \int_{\mathbb{R}^d} \mathcal{L}^* \widehat{\varphi}_{\theta,\varepsilon,\delta}(x) p_\theta(x) dx + I_\delta, \end{aligned}$$

where  $I_\delta$  refers to the second item in the second line above and note that  $|I_\delta| \leq C_\delta = \|p_\theta - p\|_{B_{r_\varepsilon+1}} (d \max_i \|b_i\|_{B_{r_\varepsilon+1}} + d^2 \max_{i,j} \|D_{ij}\|_{B_{r_\varepsilon+1}}) \|\widehat{\varphi}_{\theta,\varepsilon} - \widehat{\varphi}_{\theta,\varepsilon,\delta}\|_{H^2(B_{r_\varepsilon+1})}$ . Since  $\lim_{\delta \rightarrow 0} C_\delta \rightarrow 0$ , then  $\int_{B_{r_\varepsilon}} |p_\theta(x) - p(x)|^2 dx = \int_{\mathbb{R}^d} \mathcal{L}^* \widehat{\varphi}_{\theta,\varepsilon,\delta}(x) p_\theta(x) dx$ . Consequently, by (27), we proved that

$$\int_{\mathbb{R}^d} \mathcal{L}^* \varphi_{\theta,\varepsilon}(x) p_\theta(x) dx \leq \int_{\mathbb{R}^d} |p_\theta(x) - p(x)|^2 dx \leq \int_{\mathbb{R}^d} \mathcal{L}^* \varphi_{\theta,\varepsilon}(x) p_\theta(x) dx + \varepsilon.$$

which is analogous to (20) in the proof of Theorem (3.1). The remaining proofs are similar to that of which is analogous to (20) in the proof of Theorem (3.1).

To prove the first statement, let  $r$  be a positive constant and  $\Omega_{\theta,r} := \{\varphi \in C_c^\infty(\mathbb{R}^d) : \|\varphi - \varphi_\theta\|_{L^2(U)} \leq r\}$  represent the  $L^2$ -ball. By Assumption 4-(3) we know that the conditional distribution  $\mathbb{P}_{\theta,r,\varepsilon}(\cdot)$  is well-defined and  $\mathbb{P}_{\theta,r,\varepsilon}(\Omega_{\theta,r,\varepsilon}) = 1$ . We now can obtain a bound for the squared  $L^2$  error as follows. By replacing  $U$  with  $\mathbb{R}^d$ ,  $\mathbb{P}_{\theta,r}$  with  $\mathbb{P}_{\theta,r,\varepsilon}$ , and  $\Omega_{\theta,r}$  with  $\Omega_{\theta,r,\varepsilon}$  in (21), we immediately obtain the second inequality “ $\leq$ ” of (24). The first “ $\leq$ ” part can be proven in a similar manner as outlined in Section 3.1.

Now we turn to the second statement. The proof will also follow a similar approach as outlined in Section 3.1. For any positive constant  $r$ , we select an  $H^2$ -ball:  $\Omega'_{\theta,r,\varepsilon} := \{\varphi \in C_c^\infty(\mathbb{R}^d) : |\varphi - \widehat{\varphi}_{\theta,\varepsilon}|_{H^2(\mathbb{R}^d)} \leq r\}$ , and replace  $U$  with  $\mathbb{R}^d$ ,  $\mathbb{P}'_{\theta,r}$  with  $\mathbb{P}'_{\theta,r,\varepsilon}$ , and  $\Omega'_{\theta,r}$  with  $\Omega'_{\theta,r,\varepsilon}$  in (22). Then we obtain (25) where the constant  $C$  is given by (26).  $\square$

#### 4. NUMERICAL EXPERIMENTS

In this section, we apply WGS into four different examples: a two-dimensional system with a single mode, a two-dimensional system with two metastable states, a three-dimensional Lorenz system and a ten-dimensional problem. We use Real NVP, as mentioned in Section 2.3, to parameterize the generator  $G$  in all the examples. For each affine coupling layer in Real NVP, we use the fully connected neural networks with three hidden layers and the LeakyReLU as the activation function to parameterize the translation and scaling functions. Unless specifically stated, we use the base distribution as  $\rho(z) = \mathcal{N}(z; 0, \mathbf{I}_d)$ . The hyperparameters chosen for the boundary loss function are provided in Table 1.

In the first and second examples, we compare WGS with a method called ADDA proposed in [55], where the loss function is defined as

$$L_{\text{ADDA}} = \frac{1}{N_p} \sum_{i=1}^{N_p} |\mathcal{L} p_\theta(x_i)|^2 + \lambda L_b, \quad (28)$$

where  $\lambda L_b$  represents the same boundary condition as in our method in Table 1. In (28),  $\{x_i\}_{i=1}^{N_p}$  is sampled by  $p_{\text{data}}(x)$ , where  $p_{\text{data}}(x)$  is set as the uniform distribution in the bounded domain

TABLE 1. The choice of hyperparameters of the boundary loss function for all examples

Example	$\gamma$	$\lambda$	$c$	$x_0$	$r$
1	0.5	10	6	(0, 0)	6
2( $\varepsilon = 0.2$ )	0.5	10	6	(0, 0)	3
2( $\varepsilon = 0.1$ )	0.7	10	6	(0, 0)	3
2( $\varepsilon = 0.05$ )	0.7	10	6	(0, 0)	2
3	5	5	5	(0, 0, 25)	$30 \times 40 \times 40^1$
4	0.3	5	6	(0, 0, $\dots$ , 0)	2

<sup>1</sup> Each number represents the radius in each coordinate.

first and then set as the  $p_\theta(x)$  when adaptive technique in [55] is used. We use the same network structure as WGS to parameterize the generator  $G_\theta$  and  $p_\theta = G_{\theta\#}\rho$ .

To assess the accuracy of the learned invariant measure, we compute the relative error of the learned distribution  $p_\theta(x)$  push-forward by  $\rho(z)$ :

$$e_p = \frac{\|p_\theta(x) - p(x)\|_2}{\|p(x)\|_2}.$$

#### 4.1. Example 1: A two-dimensional system with single mode

To test the efficiency of WGS, we consider the following two-dimensional system

$$\begin{cases} dx = -(x-1)dt + \sqrt{2}dW_1, \\ dy = -(y-1)dt + \sqrt{2}dW_2. \end{cases} \quad (29)$$

The invariant distribution for this example is  $p(x) = \exp(-(x-1)^2/2 - (y-1)^2/2)/2\pi$ . We compare WGS with ADDA, which has the same network structure.

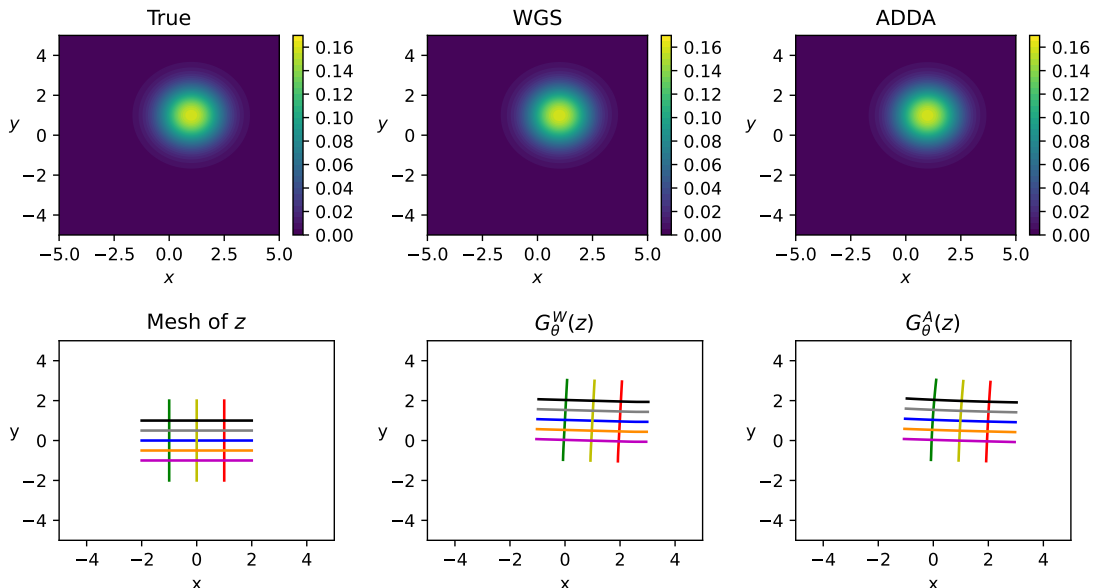


FIGURE 2. (Example 1) Contour plots of the probability density function of invariant measure  $p(x)$  (upper left),  $p_\theta^W(x)$  learned by WGS (upper middle) and  $p_\theta^A(x)$  learned by ADDA (upper right). The uniform mesh in the base space (lower left), the mesh generated by  $G_\theta^W$  (lower middle) and the mesh generated by  $G_\theta^A$  (lower right).

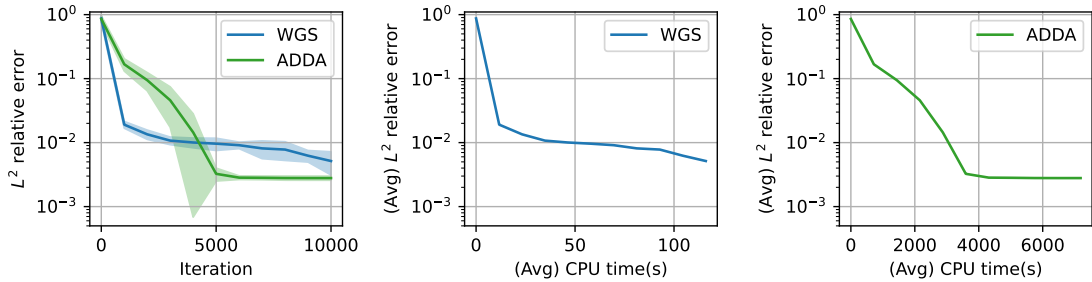


FIGURE 3. (Example 1) The left panel displays the  $L^2$  relative error versus the iteration for the learned solution  $p_\theta$  obtained from ten different runs using WGS and ADDA. The middle panel and the right panel depict the average  $L^2$  relative error against average CPU time for WGS and ADDA, respectively.

For WGS, we generated  $N = 8000$  sample points from the base distribution. We selected  $N_\varphi = 500$  test functions, and the means of these test functions were sampled from a uniform distribution in the range  $[-4, 4] \times [-4, 4]$ . The parameter  $\kappa$  was set to 1.0. For ADDA, we utilized  $N_p = 8000$  data points sampled from  $p_\theta$  during the training process. We utilize the Adam optimizer with a decay weight of learning rate to train WGS and ADDA for 10000 iterations.

Figure 2 presents a comparison between the true probability density function  $p$  (upper left), the probability density function  $p_\theta^W$  learned by WGS (upper middle), and the probability density function  $p_\theta^A$  learned by ADDA (upper right). And the uniform mesh in the base space mapped by  $G_\theta^W$  (lower middle) and  $G_\theta^A$  (lower right) are almost the same. From Figure 2, we observe that WGS and ADDA can obtain almost the same as the exact solution.

From Figure 3, We observed that WGS achieves a  $L^2$  relative error  $e_p$  approximately  $10^{-2}$  faster than ADDA. However, ADDA can achieve a smaller  $e_p$  than WGS throughout the entire iteration. It is worth noting that ADDA requires a significant amount of CPU time than WGS. Since ADDA requires the computation of the Jacobian of the generator  $G_\theta^A$  and the gradient of  $p_\theta^A$ , WGS only needs the computation of map  $G_\theta^W$ . The loss function of WGS can be computed in matrix form. We conclude that WGS strikes a reasonable balance between time and error, yielding satisfactory results.

#### 4.2. Example 2: A two-dimensional system with two metastable states

In this section, we consider the following two-dimensional dynamical system [35]

$$\begin{cases} dx = [\frac{1}{5}x(1-x^2) + y(1+\sin x)] dt + \sqrt{\frac{2}{5}\varepsilon}dW_1, \\ dy = [-y + 2x(1-x^2)(1+\sin x)] dt + \sqrt{2\varepsilon}dW_2. \end{cases} \quad (30)$$

The corresponding deterministic dynamics ( $\varepsilon = 0$ ) has two metastable states at  $x_1 = (-1, 0)^\top$  and  $x_2 = (1, 0)^\top$  and one unstable stationary point at  $x_3 = (0, 0)^\top$ . As  $\varepsilon$  becomes smaller, the barrier between two metastable states will increase.

In this example, we compare WGS with ADDA for different  $\varepsilon$ , where  $\lambda L_b$  is the same boundary condition as in our method in Table 1. We use the same network structure to parameterize the generator  $G_\theta$  and the distribution  $p_\theta = G_{\theta\#}\rho$  in WGS and ADDA.

For WGS, we generated  $N = 10000$  sample points from the base distribution for all the cases. For the experiments with  $\varepsilon = 0.2$  and  $\varepsilon = 0.1$ , we employed  $N_\varphi = 100$  different test functions and performed  $N_I = 50000$  iterations. On the other hand, for the experiment with  $\varepsilon = 0.05$ , we utilized  $N_\varphi = 500$  test functions with a batch size of  $N_\varphi^b = 100$  and executed  $N_I = 80000$  iterations to assess the performance of our algorithm. In all cases, we gradually decrease the value of  $\kappa$  from a higher value to a lower value. Specifically, for  $\varepsilon = 0.2$ , we decrease  $\kappa$  from 0.3 to 0.15. For  $\varepsilon = 0.1$ , we decrease  $\kappa$  from 0.5 to 0.15. And for  $\varepsilon = 0.05$ , we decrease  $\kappa$  from 0.2 to 0.1.

For ADDA, the initial training set is generated by the uniform distribution with range  $[-3, 3]^2$  for  $\varepsilon = 0.1$  and 0.2. For  $\varepsilon = 0.05$ , we use the uniform distribution with a range of  $[-2, 2]^2$  to obtain the initial training samples. We set  $N_p = 60000$  with a batch size of  $N_p^b = 1000$ . The number of

iterations is set at  $N_I^p = 200$ , and the number of adaptivity iterations is set at  $N_{\text{adaptive}} = 5$  for each case. We trained the transport map  $G_\theta$  using the Adam optimizer with a decaying learning rate in WGS and ADDA.

TABLE 2. Comparison of WGS and ADDA for solving the Example 2

Methods	$\varepsilon$	$e_p$	Loss <sup>1</sup>	Time/Iter <sup>2</sup>	Number of Iters
WGS	0.2	0.0422	$1.8938 \times 10^{-5}$	0.0098	$5 \times 10^4$
ADDA	0.2	0.4028	$1.0676 \times 10^{-5}$	0.1585	$6 \times 10^4$
WGS	0.1	0.0337	$1.5587 \times 10^{-5}$	0.0090	$5 \times 10^4$
ADDA	0.1	0.3893	$1.0337 \times 10^{-5}$	0.1571	$6 \times 10^4$
WGS	0.05	0.0807	$1.6816 \times 10^{-5}$	0.0095	$3.95 \times 10^5$
ADDA	0.05	0.4740	$2.6964 \times 10^{-5}$	0.1635	$6 \times 10^4$

<sup>1</sup> The loss for WGS is (12) and the loss for ADDA is (28).

<sup>2</sup> The time is the total CPU time during the training of WGS and ADDA. The iteration number for WGS is  $N_I \times N_\varphi^b$  and for ADDA is  $N_I^p \times N_p^b \times N_{\text{adaptive}}$ .

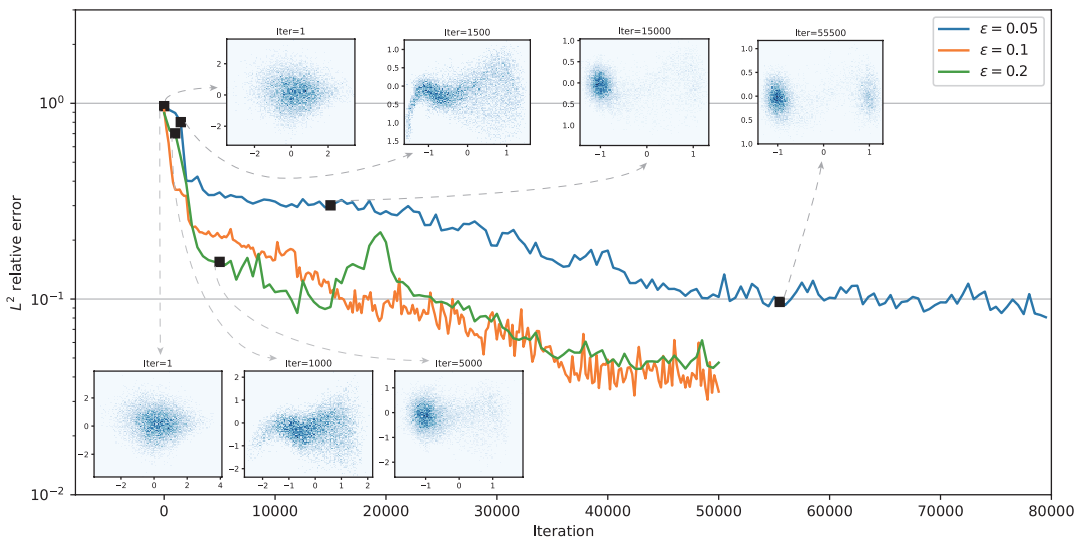


FIGURE 4. (Example 2) The  $L^2$  relative error versus the iteration for different  $\varepsilon$ . The upper panel depicts the contour plot of the sample points for specific iterations in  $\varepsilon = 0.05$ . The lower panel depicts the contour plot of the sample points for specific iterations in  $\varepsilon = 0.2$ .

As a comparison, we compute the reference solution  $p$  by the finite difference method on the domain  $\Omega = [-2, 2] \times [-3, 3]$  with a uniform mesh consisting of  $400 \times 400$  grid points for all cases. In Table 2, we present a quantitative assessment of the numerical solutions obtained using WGS and ADDA for various  $\varepsilon$  values. Compared to the ADDA method, WGS achieves a lower relative error. In the ADDA method, the generator may get stuck in a local minimum and fail to escape from it. On the other hand, WGS can move from one local minimum to another by leveraging the flexibility of the parameter  $\kappa$ . Additionally, WGS exhibits faster training in each iteration due to the absence of Jacobian and gradient computations for  $p_\theta$ . Figure 4 shows the  $L^2$  relative error  $e_p$  versus the iteration for different  $\varepsilon$ . WGS demonstrates the capability to rapidly capture two metastable states within the system, indicating its effective utilization of the generator's flexibility. However, we should also note that WGS may take much more time to converge when the temperature is low. In Figure 5, we utilize WGS and ADDA to generate 2000 sample data

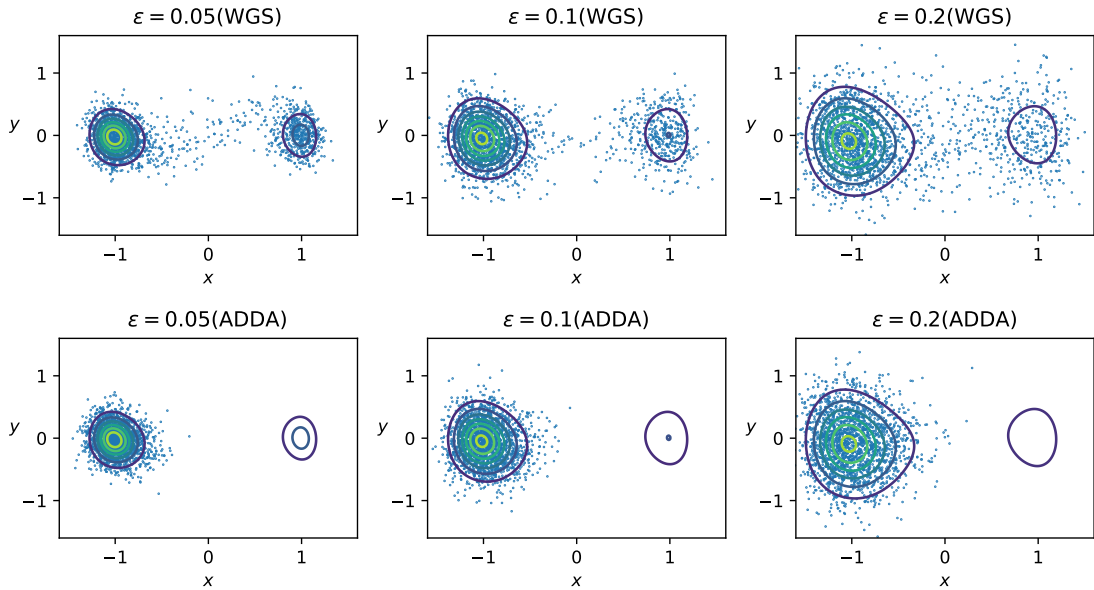


FIGURE 5. (Example 2) The data points displayed on the contour plot represent the sample points obtained through the application of the trained WGS and ADDA methods for  $\varepsilon = 0.05, 0.1$  and  $0.2$ .

points for different  $\varepsilon$  values in Example 2. These points are then plotted on the contour plot of the true probability density function. It is worth noting that while ADDA may remain trapped in the metastable basin around  $x_1$ , WGS demonstrates the ability to explore the entire domain.

Figure 6 showcases the comparison between the reference probability density function  $p$  (upper panel), the probability density function  $p_\theta^W$  learned by WGS (middle panel), and the probability density function  $p_\theta^P$  learned by ADDA (lower panel), for all cases. The results clearly demonstrate that our algorithm is effective in capturing the characteristics of the distribution in both high and low temperature regimes, compared with ADDA.

### 4.3. Example 3: Lorenz system

In this section, we apply the WGS to the Lorenz system, which captures complex atmospheric convection. The Lorenz system exhibits chaotic behaviour, which is sensitive to initial conditions, known as the butterfly effect. The dynamical equations of the Lorenz system in the presence of noise in the three-dimensional space are given by

$$\begin{cases} dx = \beta_1(y - x)dt + \sqrt{2\varepsilon}dW_1, \\ dy = (x(\beta_2 - z) - y)dt + \sqrt{2\varepsilon}dW_2, \\ dz = (xy - \beta_3z)dt + \sqrt{2\varepsilon}dW_3, \end{cases} \quad (31)$$

where  $W = (W_1, W_2, W_3)^\top$  is a three-dimensional white noise, and the diffusion matrix  $D = 2\varepsilon\mathbf{I}_3$  denotes the three-dimensional identity matrix. We take the parameters  $\beta_1 = 10, \beta_2 = 28$  and  $\beta_3 = 8/3$ . Under these parameter values, the shape of the attractor in the deterministic system resembles a butterfly. We take the parameter  $\varepsilon = 20$ .

In this case, we incorporate 12 affine coupling layers within the Real NVP architecture, each consisting of a three-layer neural network. The base distribution is set as  $\rho(z) = \mathcal{N}(0, 20\mathbf{I}_d)$ . The training process encompasses  $N_I = 7500$  iterations, and the dataset comprises  $N = 10,000$  sample points. We select  $N_\varphi = 10,000$  with a batch size of 1000. We set  $\eta = 5$  and  $\kappa = 5$  throughout the training phase. The learning rate is set to 0.0002.

To validate the accuracy of our method, we use the Euler-Maruyama method to run the SDE to estimate the probability density function  $p$  of the invariant measure. In the Euler-Maruyama method, we first sample 1000 points uniformly from  $[-25, 25] \times [-30, 30] \times [-10, 60]$ . We then simulate 1000 trajectories over a sufficient enough long time  $T = 10^5$  with time step  $\delta t = 10^{-3}$ .

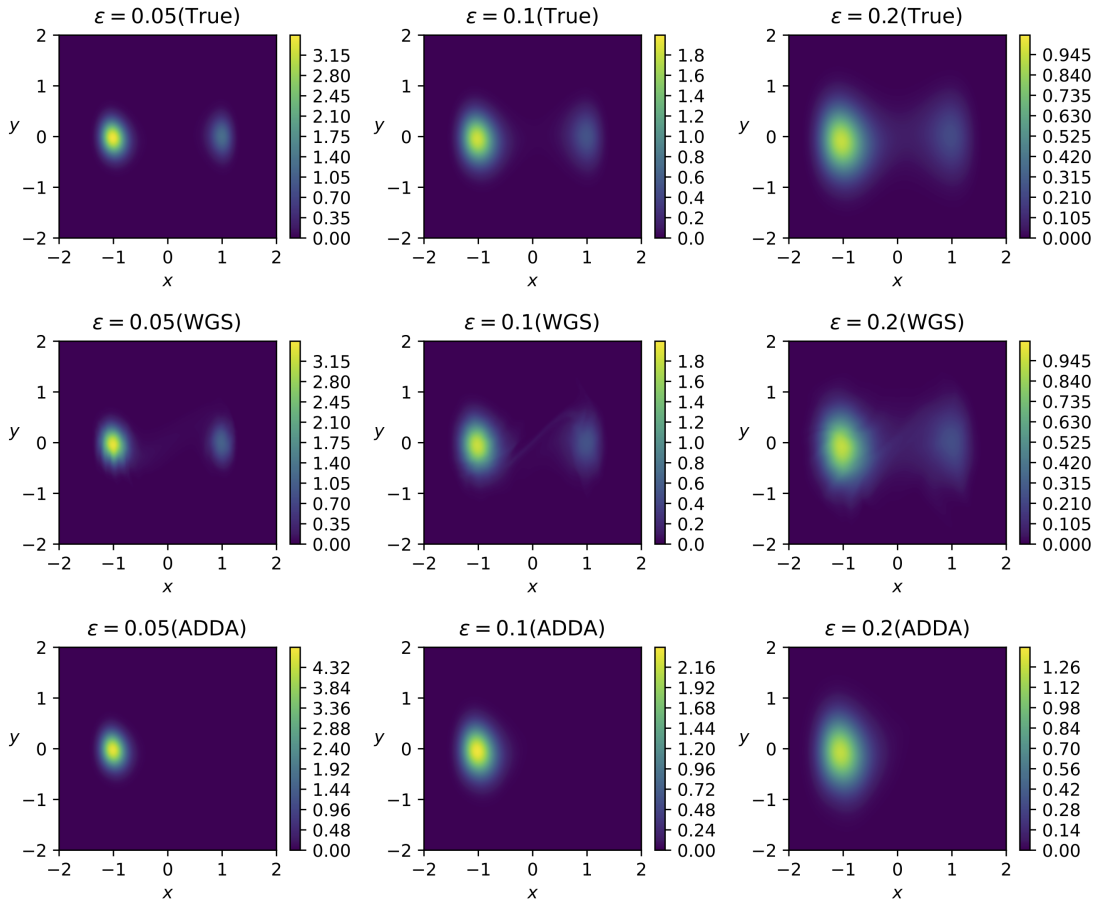


FIGURE 6. (Example 2) Contour plots of the probability density function of invariant measure  $p(x)$ , where  $p(x)$  is the finite difference solution of the FP equation (top),  $p_\theta^W(x)$  learned by WGS (middle) and  $p_\theta^P(x)$  learned by ADDA for  $\varepsilon = 0.05$  (left),  $\varepsilon = 0.1$  (middle) and  $\varepsilon = 0.2$  (right)

After reaching a specific time  $T_0 = 100$ , we will save the running data points every 1000 iterations. To estimate the probability density function  $p$ , we refine a mesh with  $[-30, 30] \times [-40, 40] \times [-10, 60]$  and then compute the number of sample data points in each bin. For comparison, we use the learned generator  $G_\theta$  to sample data points and then estimate the probability density function  $\hat{p}_\theta$  by the same refined mesh.

In Figure 7, we choose two random data points and use the black arrow to plot the generator map  $G_\theta$ . In Figure 8, we plot the marginal probability density function  $p(x, y)$ ,  $p(x, z)$  and  $p(y, z)$  estimated by the Monte Carlo method and the learned marginal probability density function  $\hat{p}_\theta(x, y)$ ,  $\hat{p}_\theta(x, z)$  and  $\hat{p}_\theta(y, z)$ . The relative  $L^2$  error between  $p$  and  $\hat{p}_\theta$  is  $e_p = 0.157$ .

#### 4.4. Example 4: A ten-dimensional problem

In this example, we test WGS in a ten-dimensional problem to show the effectiveness of WGS. The system is obtained by coupling the following five identical and independent two-dimensional systems [35]

$$\begin{cases} dy_{2i-1} = (-y_{2i-1} + y_{2i}(1 + \sin y_{2i-1}))dt + \sqrt{2\varepsilon}dW_{2i-1}, \\ dy_{2i} = (-y_{2i} - y_{2i-1}(1 + \sin y_{2i-1}))dt + \sqrt{2\varepsilon}dW_{2i}, \quad 1 \leq i \leq 5 \end{cases} \quad (32)$$

where  $W = (W_1, W_2, \dots, W_{10})^T$  is a  $10d$  Brownian motion. The ten-dimensional dynamics is coupled by the transformation of  $x = By \in \mathbb{R}^{10}$ , where  $B \in \mathbb{R}^{10 \times 10}$  is a given matrix and

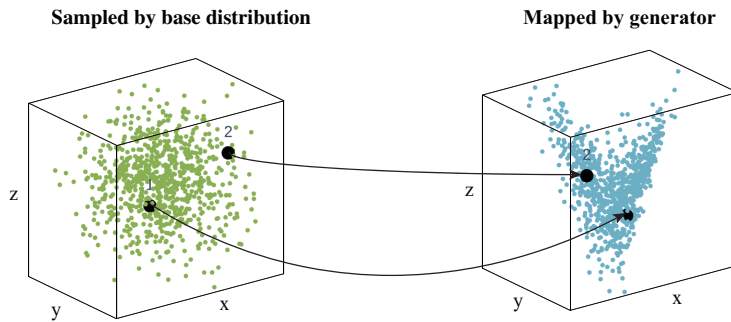


FIGURE 7. (Example 3) The generator map  $G_\theta$  trained by WGS. The left panel shows the data points sampled by the base distribution and the right panel shows the data points mapped by the generator map  $G_\theta$ .

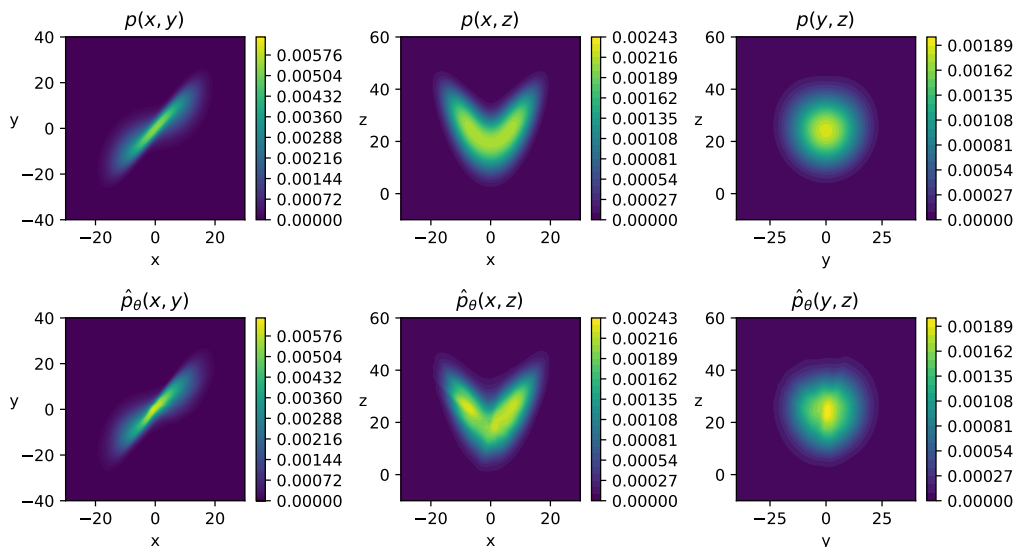


FIGURE 8. (Example 3) Contour plots of the marginal probability density function  $p(x, y)$ ,  $p(x, z)$  and  $p(y, z)$  estimated using the Monte Carlo method (upper) and the learned marginal probability density function  $\hat{p}_\theta(x, y)$ ,  $\hat{p}_\theta(x, z)$  and  $\hat{p}_\theta(y, z)$  computed by WGS.

$y = (y_1, \dots, y_{10})$ . Then, the dynamic of the variable  $x$  is governed by the equation

$$dx = f(x)dt + \sqrt{2\varepsilon}BdW. \quad (33)$$

where the force  $f$  can be determined by the transformation  $x = By$ . The matrix  $B = [b_{ij}]$  is given by

$$b_{ij} = \begin{cases} 0.8, & \text{for } i = j = 2k - 1, 1 \leq k \leq 5 \\ 1.25, & \text{for } i = j = 2k, 1 \leq k \leq 5 \\ -0.5, & \text{for } j = i + 1, 1 \leq i \leq 9 \\ 0, & \text{otherwise} \end{cases}$$

and we set  $\varepsilon = 0.1$ . By the transformation of  $x = By$ , we can use the stationary Fokker–Planck equation to show that the invariant distribution of the system (33) is given by

$$p(x) = \prod_{i=1}^5 p_0(y_{2i-1}, y_{2i}),$$

where  $(y_1, \dots, y_{10}) = B^{-1}x$  and  $p_0$  is the invariant distribution of the  $2d$  system (32) can be computed by the finite difference method.

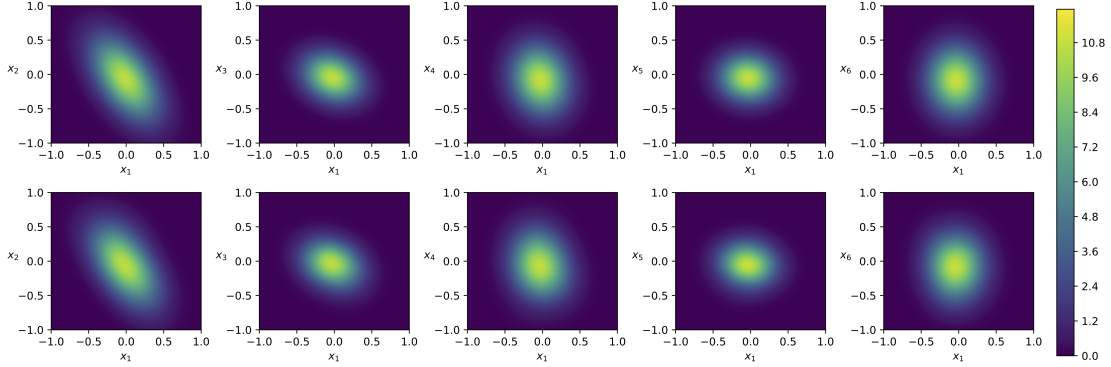


FIGURE 9. (Example 4) Cross sections of the FD solution  $p$  (top) and the learned solution  $p_\theta$  push forward by  $G_\theta$  (bottom) on the  $x_1$ - $x_i$  plane,  $2 \leq i \leq 6$ , where the other coordinates are set to zero.

In this case, we incorporate 12 affine coupling layers within the Real NVP architecture, each consisting of a three-layer neural network. The training process encompasses  $N_I = 100$  iterations, and the dataset comprises  $N = 30,000$  sample points. We select  $N_\varphi = 30,000$  with a batch size of 100. Throughout the training phase, the width hyper-parameter  $\kappa$  was gradually reduced from 0.8 to 0.4. The learning rate is set to 0.0001.

For each of the five planes depicted in the columns of Figure 9, we compute the relative error by comparing the learned probability density function, denoted as  $p_\theta$ , with its projection onto the two-dimensional plane while keeping the remaining coordinates fixed at 0. The corresponding relative errors for the five planes are 0.0249, 0.0265, 0.0456, 0.0477, and 0.0322, respectively. The results demonstrate a satisfactory agreement between the two solutions across all five cross sections, encompassing both high-probability and low-probability regions within this high-dimensional system.

We remark that using the  $\kappa$  gradually from high to low can perform better. In Figure 10, we compare with  $\kappa = 0.8$  and gradually reduce  $\kappa$  from 0.8 to 0.4 by five different runs of our algorithm. We observe that different choices of  $\kappa$  can influence the convergence rate of the method, and gradually reducing  $\kappa$  can perform better than using only the same  $\kappa$  during the algorithm’s training.

## 5. CONCLUSION AND OUTLOOK

In this paper, we have presented a novel method called weak generative sampler (WGS) for sampling the invariant measure of diffusion processes. The WGS method utilizes the weak form of the SFPE, eliminating the need for Jacobian computations and resulting in significant computational savings. By selecting test functions based on data-driven approaches, the WGS effectively identifies all metastable states in the system. The current randomization strategy of the Gaussian kernel test function may suggest a new type of adaptive strategy beyond the current mainstream adaptive methods of PINN, which will be explored as a future work. When the equation contains certain parameters, for example the noise intensity  $\varepsilon$ , the current WGS can be naturally generalized to train a parametric generative map  $G_\theta(z, \varepsilon)$  from  $\mathbb{R}^{d+1}$  to  $\mathbb{R}^d$  by wrapping our randomized weak loss function with one more average over the sampled values of the parameters  $\varepsilon$ . We anticipate further exploration of WGS’s applications to time-dependent Fokker–Planck equations and McKean-Vlasov problems, expanding its potential for more general scenarios.

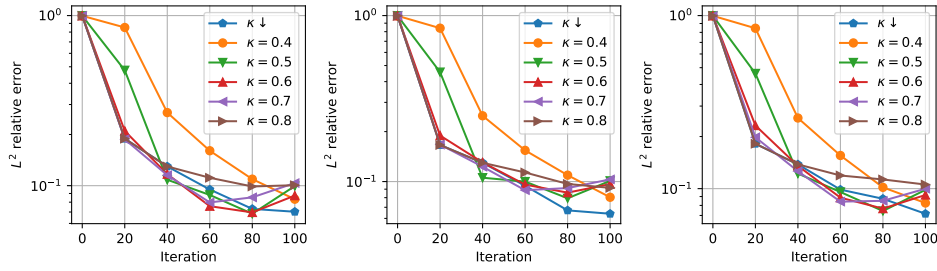


FIGURE 10. (Example 4) Comparison with different choice of  $\kappa$  by the relative error for the cross-section of the learned solution  $p_\theta$  on the  $x_1$ - $x_2$  plane (left),  $x_1$ - $x_4$  plane (middle),  $x_1$ - $x_6$  plane (right), where the other coordinates are set to zero.  $\kappa \downarrow$  denotes that  $\kappa$  gradually decrease from 0.8 to 0.4.

## APPENDIX

### APPENDIX A. CONSTRUCTION OF PROBABILITY MEASURES ON TEST FUNCTION SPACES

We show in this Appendix the existences of the probability measures required in Assumption 2 and 4, by constructing such a probability measure on the different test function spaces. We emphasize that the construction here only to show the existence in theoretic probability, not the practical data-driven construction of the test function in our Algorithm 1, which certainly satisfies Assumption 2 and 4.

We first consider the Sobolev space  $(H^2(\mathbb{R}^d), \langle \cdot, \cdot \rangle)$ , which is a separate Hilbert space, where the inner product is given by

$$\langle f, g \rangle = \sum_{|\alpha| \leq 2} \int_{\mathbb{R}^d} (\partial^\alpha f)(\partial^\alpha g) dx.$$

We denote by  $L(H^2(\mathbb{R}^d))$  the Banach algebra of all continuous linear operators from  $H^2(\mathbb{R}^d)$  to  $H^2(\mathbb{R}^d)$ , by  $L^+(H^2(\mathbb{R}^d))$  the set of all  $T \in L(H^2(\mathbb{R}^d))$  which are symmetric ( $\langle Tf, g \rangle = \langle f, Tg \rangle$ ,  $f, g \in H^2(\mathbb{R}^d)$ ), and by  $L_1^+(H^2(\mathbb{R}^d))$  the set of all operators  $Q \in L^+(H^2(\mathbb{R}^d))$  of trace class that is such that  $\text{Tr } Q := \sum_{k=1}^{\infty} \langle Qe_k, e_k \rangle < \infty$  for one complete orthonormal system  $(e_k)$  in  $H^2(\mathbb{R}^d)$ . We know that [7, Section 1.5 & Chapter 9], there exist non-degenerate (i.e.,  $\text{Ker}(Q) = \{f \in H^2(\mathbb{R}^d) : Qf = 0\} = \{0\}$ ) Gaussian measures on  $(H^2(\mathbb{R}^d), \|\cdot\|_{H^2(\mathbb{R}^d)})$  where the associated norm  $\|\cdot\|_{H^2(\mathbb{R}^d)}$  is

$$\|f\|_{H^2(\mathbb{R}^d)} = \sum_{|\alpha| \leq 2} \left( \int_{\mathbb{R}^d} |\partial^\alpha f|^2 dx \right)^{\frac{1}{2}}.$$

Let  $\mathcal{N}_{0, Q^*}$  be such a Gaussian measure with mean 0 and covariance  $Q^* \in L_1^+(H^2(\mathbb{R}^d))$ . There exists a sequence of non-negative numbers  $(\lambda_k)$  such that

$$Q^* e_k = \lambda_k e_k, \quad k \in \mathbb{N}.$$

For any  $f \in H^2(\mathbb{R}^d)$  we set  $f_k = \langle f, e_k \rangle$ ,  $k \in \mathbb{N}$ . Now let us consider the natural isomorphism  $\gamma$  between  $H^2(\mathbb{R}^d)$  and the Hilbert space  $l^2$  of all sequence  $(f_k)$  of real numbers such that

$$\sum_{k=1}^{\infty} |f_k|^2 < \infty,$$

defined by

$$H^2(\mathbb{R}^d) \rightarrow l^2, \quad f \mapsto \gamma(f) = (f_k).$$

And we shall identify  $H^2(\mathbb{R}^d)$  with  $l^2$  and thus the corresponding probability measure for  $\mathcal{N}_{0, Q^*}$  is the following product measure

$$\mu := \prod_{k=1}^{\infty} \mathcal{N}_{0, \lambda_k},$$

where  $\mathcal{N}_{0,\lambda_k}$  is the Gaussian measure in  $\mathbb{R}$  with mean 0 and variance  $\lambda_k$ . Though  $\mu$  is defined on  $\mathbb{R}^\infty := \times_{k=1}^\infty \mathbb{R}$ , it is concentrate in  $l^2$  [7, Proposition 1.11]. However, every bounded Borel set, e.g. unit ball, in  $\mathcal{B}(H^2(\mathbb{R}^d))$  under such Gaussian measure  $\mu$  has zero mass. Now we turn to its projection. For any given  $n \in \mathbb{Z}$ , we consider the projection mapping  $P_n : H^2(\mathbb{R}^d) \rightarrow P_n(H^2(\mathbb{R}^d))$  defined as

$$P_n f = \sum_{k=1}^n \langle f, e_k \rangle e_k, \quad f \in H^2(\mathbb{R}^d).$$

Obviously we have  $\lim_{n \rightarrow \infty} P_n f = f$  for all  $f \in H^2(\mathbb{R}^d)$ .

Since the test function space  $C_c^\infty(\mathbb{R}^d)$  is dense in  $H^2(\mathbb{R}^d)$ , so  $\mathcal{B}(H^2(\mathbb{R}^d)) \cap C_c^\infty(\mathbb{R}^d)$  is a Borel  $\sigma$ -field on  $C_c^\infty(\mathbb{R}^d)$ , that is for every  $A \in C_c^\infty(\mathbb{R}^d)$  there exists  $\tilde{A} \in \mathcal{B}(H^2(\mathbb{R}^d))$  such that  $A = \tilde{A} \cap C_c^\infty(\mathbb{R}^d)$ . For a fixed  $n \in \mathbb{Z}$ , define the measure  $\mathbb{P}$  as

$$\mathbb{P}(A) := \left( \prod_{k=1}^n \mathcal{N}_{0,\lambda_k} \right) (P_n(\tilde{A})), \quad \forall A \in \mathcal{B}(H^2(\mathbb{R}^d)) \cap C_c^\infty(\mathbb{R}^d).$$

It is easy to see  $\mathbb{P}$  is a probability measure on  $(C_c^\infty(\mathbb{R}^d), \mathcal{B}(H^2(\mathbb{R}^d)) \cap C_c^\infty(\mathbb{R}^d))$  satisfying the Assumption 4-(3) due to the following property.

**Proposition A.1.** *For any given  $n \in \mathbb{Z}$ ,  $r > 0$  and  $r_0 > 0$ , we have*

$$\inf_{f \in \bar{B}(0,r)} \left( \prod_{k=1}^n \mathcal{N}_{0,\lambda_k} \right) (P_n(\bar{B}_{H^2(\mathbb{R}^d)}(f, r_0))) > 0,$$

where  $\bar{B}_{H^2(\mathbb{R}^d)}(f, r_0) = \{g \in H^2(\mathbb{R}^d) : \|f - g\|_{H^2(\mathbb{R}^d)} \leq r_0\}$  is the closed ball centered at  $f$  and with  $r_0$  radius in  $H^2(\mathbb{R}^d)$ .

*Proof.* Note that,  $\mathcal{N}_{0,Q^*}$  is a nondegenerate Gaussian measure on  $H^2(\mathbb{R}^d)$ , and

$$\begin{aligned} \left( \prod_{k=1}^n \mathcal{N}_{0,\lambda_k} \right) (P_n(\bar{B}(f, r_0))) &= \left( \prod_{k=1}^n \mathcal{N}_{0,\lambda_k} \right) (P_n(\{g \in \mathbb{R}^\infty : |f - g|_{l^2}^2 \leq r_0\})) \\ &= \left( \prod_{k=1}^n \mathcal{N}_{0,\lambda_k} \right) \left( P_n \left\{ g \in \mathbb{R}^\infty : \sum_{k=1}^\infty |(f - g)_k|^2 \leq r_0 \right\} \right) \\ &= \left( \prod_{k=1}^n \mathcal{N}_{0,\lambda_k} \right) \{g \in \mathbb{R}^n : f_k - \sqrt{r_0} \leq g_k \leq f_k + \sqrt{r_0}\} \\ &= \prod_{k=1}^n \mathcal{N}_{0,\lambda_k} ([f_k - \sqrt{r_0}, f_k + \sqrt{r_0}]) > 0. \end{aligned}$$

Also note that the 1-dimensional Gaussian distribution is continuous, and thus  $(\prod_{k=1}^n \mathcal{N}_{0,\lambda_k}) (P_n(\bar{B}(\cdot, r_0)))$  is a continuous function on  $(H^2(\mathbb{R}^d), \|\cdot\|_{H^2(\mathbb{R}^d)})$ ,  $(\prod_{k=1}^n \mathcal{N}_{0,\lambda_k}) (P_n(\bar{B}(\cdot, r_0))) : H^2(\mathbb{R}^d) \rightarrow [0, 1]$ . Thus the infimum value of  $(\prod_{k=1}^n \mathcal{N}_{0,\lambda_k}) (P_n(\bar{B}(\cdot, r_0)))$  on any closed ball can be achieved and is nonnegative. In particular,

$$\inf_{f \in \bar{B}(0,r)} \left( \prod_{k=1}^n \mathcal{N}_{0,\lambda_k} \right) (P_n(\bar{B}(f, r_0))) \geq \prod_{k=1}^n \mathcal{N}_{0,\lambda_k} ([r - \sqrt{r_0}, r + \sqrt{r_0}]) > 0,$$

□

Note that  $L^2(\mathbb{R}^d)$  is also a separable Hilbert space and its elements can also be approximated by sequences of  $C_c^\infty(\mathbb{R}^d)$ , and thus in a similar way as before we can find a nondegenerate Gaussian measure on  $L^2(\mathbb{R}^d)$  and construct a probability measure  $\mathbb{P}$  based on it and its projection on space  $C_c^\infty(\mathbb{R}^d)$ .

Next, let us consider the construction of  $\mathbb{P}$  for test functions restricted in  $B_{r_\varepsilon}$ . As similar with before, the Sobolev space  $H^2(B_{r_\varepsilon})$  is a separate Hilbert space and thus there exist Gaussian measure on  $(H^2(B_{r_\varepsilon}), \mathcal{B}(H^2(B_{r_\varepsilon})), \|\cdot\|_{H^2(B_{r_\varepsilon})})$ . We choose one of any non-degenerate Gaussian measures and denote it by  $\mathcal{N}$ . We know that every function in  $H^2(B_{r_\varepsilon})$  can be approximated by a sequence of functions of  $C^\infty(\bar{B}_{r_\varepsilon})$ . Let  $C^{\infty*}(B_{r_\varepsilon}) := \{\varphi|_{B_{r_\varepsilon}} : \varphi \in C^\infty(\bar{B}_{r_\varepsilon})\}$ , then  $C^{\infty*}(B_{r_\varepsilon})$  is dense in  $H^2(B_{r_\varepsilon})$ . Equip the space  $C^{\infty*}(B_{r_\varepsilon})$  with the Borel  $\sigma$ -field  $\mathcal{B}(H^2(B_{r_\varepsilon})) \cap C^{\infty*}(B_{r_\varepsilon})$ .

For every  $A \in \mathcal{B}(H^2(B_{r_\varepsilon})) \cap C^{\infty*}(B_{r_\varepsilon})$  there exists  $\tilde{A} \in \mathcal{B}(H^2(B_{r_\varepsilon}))$  such that the closure of  $A$  is identical to  $\tilde{A}$ .

Define a measure  $\mathbb{P}_0$  on the  $\sigma$ -field  $\mathcal{B}(H^2(B_{r_\varepsilon})) \cap C^{\infty*}(B_{r_\varepsilon})$  by

$$\mathbb{P}_0(A) := \mathcal{N}(\tilde{A}), \quad \forall A \in \mathcal{B}(H^2(B_{r_\varepsilon})) \cap C^{\infty*}(B_{r_\varepsilon}).$$

It is easy to see  $\mathbb{P}_0$  is a probability measure on  $(C^{\infty*}(B_{r_\varepsilon}), \mathcal{B}(H^2(B_{r_\varepsilon})) \cap C^{\infty*}(B_{r_\varepsilon}))$ .

By the Whitney extension theorem, [60, Theorem I], we know that for every function in  $C^\infty(\bar{B}_{r_\varepsilon})$  there exists an extension of it in  $C^\infty(\mathbb{R}^d)$ . So we can use the extension to construct an element belonging to  $C_c^\infty(\mathbb{R}^n)$  by truncating the extension on a bigger domain and operating it by a mollifier as before. In converse every element in  $C_c^\infty(\mathbb{R}^n)$  restricted on  $\bar{B}_{r_\varepsilon}$  belongs to  $C^\infty(\bar{B}_{r_\varepsilon})$ . And we also know that every element of  $C^\infty(\bar{B}_{r_\varepsilon})$  restricted on  $B_{r_\varepsilon}$  belongs to  $H^2(B_{r_\varepsilon})$ .

Now we define an equivalence relation “ $\sim$ ” in  $C_c^\infty(\mathbb{R}^d)$  as follows:  $\varphi \sim \psi$  if  $\varphi|_{B_{r_\varepsilon}} = \psi|_{B_{r_\varepsilon}}$ , i.e.,  $\varphi(x) = \psi(x)$  when  $x \in B_{r_\varepsilon}$ .

Thus the test function space  $C_c^\infty(\mathbb{R}^d)$  under relation  $\sim$  and the  $H^2(B_{r_\varepsilon})$  norm defines a topological space having the same structure of  $(C^{\infty*}(B_{r_\varepsilon}), \mathcal{B}(H^2(B_{r_\varepsilon})) \cap C^{\infty*}(B_{r_\varepsilon}))$ . Denote such topological space as  $(C_c^\infty(\mathbb{R}^d), \mathcal{B}(C_c^\infty(\mathbb{R}^d), \sim, \|\cdot\|_{H^2(B_{r_\varepsilon})}))$ . For any  $A' \in \mathcal{B}(C_c^\infty(\mathbb{R}^d), \sim, \|\cdot\|_{H^2(B_{r_\varepsilon})})$  there exists  $A \in \mathcal{B}(H^2(B_{r_\varepsilon})) \cap C^{\infty*}(B_{r_\varepsilon})$  such that

$$A' = \{\varphi \in C_c^\infty(\mathbb{R}^d) : \varphi|_{B_{r_\varepsilon}} \in A\},$$

also in converse way, for any  $A \in \mathcal{B}(H^2(B_{r_\varepsilon})) \cap C^{\infty*}(B_{r_\varepsilon})$  there exists  $A' \in \mathcal{B}(C_c^\infty(\mathbb{R}^d), \sim, \|\cdot\|_{H^2(B_{r_\varepsilon})})$  such that

$$A = \{\varphi|_{B_{r_\varepsilon}} \in C^{\infty*}(B_{r_\varepsilon}) : \varphi \in A'\}.$$

Define a measure  $\mathbb{P}$  on the space  $C_c^\infty(\mathbb{R}^d)$  as follows,

$$\mathbb{P}(A') := \mathbb{P}_0(A), \quad \forall A' \in \mathcal{B}(C_c^\infty(\mathbb{R}^d), \sim, \|\cdot\|_{H^2(B_{r_\varepsilon})}). \quad (34)$$

Then we obtain the measure satisfying the assumptions we need.

Finally, we can conclude that the probability measure  $\mathbb{P}$  on  $C_0^\infty(U)$ , as discussed in Section 3.1, can be constructed in a similar manner. We consider the space  $H^2(V)$ , where  $V$  is a strict subset of  $U$ . Then the rest of the construction follows in the same way as before.

## REFERENCES

- [1] Vladimir I. Bogachev, Nicolai V. Krylov, Michael Röckner, and Stanislav V. Shaposhnikov. *Fokker–Planck–Kolmogorov Equations*. AMS, London, 2015.
- [2] Joan Bruna, Benjamin Peherstorfer, and Eric Vanden-Eijnden. Neural Galerkin schemes with active learning for high-dimensional evolution equations. *Journal of Computational Physics*, 496:112588, 2024.
- [3] Axel Brünger, Charles L Brooks III, and Martin Karplus. Stochastic boundary conditions for molecular dynamics simulations of ST2 water. *Chem. Phys. Lett.*, 105(5):495–500, 1984.
- [4] Xiang Cheng, Niladri S. Chatterji, Peter L. Bartlett, and Michael I. Jordan. Underdamped Langevin MCMC: A non-asymptotic analysis. In Sébastien Bubeck, Vianney Perchet, and Philippe Rigollet, editors, *Proceedings of the 31st Conference On Learning Theory*, volume 75 of *Proceedings of Machine Learning Research*, pages 300–323. PMLR, 2018.
- [5] Will Cousins and Themistoklis P Sapsis. Reduced-order precursors of rare events in unidirectional nonlinear water waves. *Journal of Fluid Mechanics*, 790:368–388, 2016.
- [6] Tiangang Cui, Hans De Sterck, Alexander D Gilbert, Stanislav Polishchuk, and Robert Scheichl. Multilevel Monte Carlo Methods for Stochastic Convection–Diffusion Eigenvalue Problems. *Journal of Scientific Computing*, 99(3):1–34, 2024.
- [7] Giuseppe Da Prato. *An introduction to infinite-dimensional analysis*. Springer Science & Business Media, 2006.
- [8] Arnak S. Dalalyan and Lionel Riou-Durand. On sampling from a log-concave density using kinetic Langevin diffusions. *Bernoulli*, 26(3):1956–1988, 2020.
- [9] Eric Darve and Andrew Pohorille. Calculating free energies using average force. *The Journal of chemical physics*, 115(20):9169–9183, 2001.
- [10] Eric Darve, Jose Solomon, and Amirali Kia. Computing generalized Langevin equations and generalized Fokker–Planck equations. *Proceedings of the National Academy of Sciences*, 106(27):10884–10889, 2009.
- [11] Laurent Dinh, Jascha Sohl-Dickstein, and Samy Bengio. Density estimation using Real NVP. In *International Conference on Learning Representations*, 2016.
- [12] Conor Durkan, Artur Bekasov, Iain Murray, and George Papamakarios. Neural spline flows. *Advances in neural information processing systems*, 32, 2019.
- [13] Weinan E and Bing Yu. The Deep Ritz Method: A Deep Learning-Based Numerical Algorithm for Solving Variational Problems. *Commun. Math. Stat.*, 6(1):1–12, 2018.

- [14] Donald L. Ermak and Helen Buckholz. Numerical integration of the Langevin equation: Monte Carlo simulation. *J. Comput. Phys.*, 35(2):169–182, 1980.
- [15] Lawrence C Evans. *Partial differential equations*, volume 19. American Mathematical Society, 2022.
- [16] Francis Filbet and Lorenzo Pareschi. A numerical method for the accurate solution of the Fokker–Planck–Landau equation in the nonhomogeneous case. *Journal of Computational Physics*, 179(1):1–26, 2002.
- [17] Marylou Gabrié, Grant M. Rotskoff, and Eric Vanden-Eijnden. Adaptive Monte Carlo augmented with normalizing flows. *Proceedings of the National Academy of Sciences*, 119(10):e2109420119, March 2022.
- [18] Zhiwei Gao, Tao Tang, Liang Yan, and Tao Zhou. Failure-informed adaptive sampling for PINNs, part II: combining with re-sampling and subset simulation. *Communications on Applied Mathematics and Computation*, pages 1–22, 2023.
- [19] David Gilbarg and Neil S Trudinger. *Elliptic partial differential equations of second order*. Springer, 1977.
- [20] Hagen Gilding and Tony Shardlow. SDELab: A package for solving stochastic differential equations in MATLAB. *Journal of computational and applied mathematics*, 205(2):1002–1018, 2007.
- [21] Ian Goodfellow, Jean Pouget-Abadie, Mehdi Mirza, Bing Xu, David Warde-Farley, Sherjil Ozair, Aaron Courville, and Yoshua Bengio. Generative adversarial nets. *Advances in neural information processing systems*, 27, 2014.
- [22] Niels Grønbech-Jensen and Oded Farago. A simple and effective Verlet-type algorithm for simulating Langevin dynamics. *Mol. Phys.*, 111(8):983–991, 2013.
- [23] Yiqi Gu, John Harlim, Senwei Liang, and Haizhao Yang. Stationary density estimation of Itô diffusions using deep learning. *SIAM Journal on Numerical Analysis*, 61(1):45–82, 2023.
- [24] Jiayue Han, Zhiqiang Cai, Zhiyou Wu, and Xiang Zhou. Residual-Quantile Adjustment for Adaptive Training of Physics-informed Neural Network. In *2022 IEEE International Conference on Big Data (Big Data)*, pages 921–930, 2022.
- [25] Jiequn Han, Arnulf Jentzen, and Weinan E. Solving high-dimensional partial differential equations using deep learning. *Proceedings of the National Academy of Sciences*, 115(34):8505–8510, 2018.
- [26] Jonathan Ho, Xi Chen, Aravind Srinivas, Yan Duan, and Pieter Abbeel. Flow++: Improving flow-based generative models with variational dequantization and architecture design. In *International Conference on Machine Learning*, pages 2722–2730. PMLR, 2019.
- [27] Martin Huttenhaller and Arnulf Jentzen. *Numerical approximations of stochastic differential equations with non-globally Lipschitz continuous coefficients*, volume 236. American Mathematical Society, 2015.
- [28] Priyank Jaini, Kira A Selby, and Yaoliang Yu. Sum-of-squares polynomial flow. In *International Conference on Machine Learning*, pages 3009–3018. PMLR, 2019.
- [29] Diederik P Kingma and Max Welling. Auto-encoding variational bayes. In *The second International Conference on Learning Representations*, 2014.
- [30] Ivan Kobyzev, Simon JD Prince, and Marcus A Brubaker. Normalizing flows: An introduction and review of current methods. *IEEE transactions on pattern analysis and machine intelligence*, 43(11):3964–3979, 2020.
- [31] Aditi Krishnapriyan, Amir Gholami, Shandian Zhe, Robert Kirby, and Michael W Mahoney. Characterizing possible failure modes in physics-informed neural networks. *Advances in Neural Information Processing Systems*, 34:26548–26560, 2021.
- [32] Pankaj Kumar and S Narayanan. Solution of Fokker–Planck equation by finite element and finite difference methods for nonlinear systems. *Sadhana*, 31:445–461, 2006.
- [33] Benedict Leimkuhler and Charles Matthews. Rational construction of stochastic numerical methods for molecular sampling. *Appl. Math. Res. eXpress*, 2013(1):34–56, 2013.
- [34] Bo Lin, Qianxiao Li, and Weiqing Ren. Computing the invariant distribution of randomly perturbed dynamical systems using deep learning. *Journal of Scientific Computing*, 91(3):77, 2022.
- [35] Bo Lin, Qianxiao Li, and Weiqing Ren. Computing high-dimensional invariant distributions from noisy data. *Journal of Computational Physics*, 474:111783, 2023.
- [36] Jianfeng Lu and Eric Vanden-Eijnden. Methodological and Computational Aspects of Parallel Tempering Methods in the Infinite Swapping Limit. *J Stat Phys*, January 2019.
- [37] Liwei Lu, Zhijun Zeng, Yan Jiang, Yi Zhu, and Pipi Hu. Weak Collocation Regression method: fast reveal hidden stochastic dynamics from high-dimensional aggregate data. *Journal of Computational Physics*, 502:112799, 2024.
- [38] Zhiping Mao and Xuhui Meng. Physics-informed neural networks with residual/gradient-based adaptive sampling methods for solving partial differential equations with sharp solutions. *Applied Mathematics and Mechanics*, 44(7):1069–1084, 2023.
- [39] Youssef Marzouk, Tarek Moselhy, Matthew Parno, and Alessio Spantini. Sampling via measure transport: An introduction. *Handbook of uncertainty quantification*, 1:2, 2016.
- [40] Mathias Rousset, Gabriel Stoltz, and Tony Lelièvre. *Free Energy Computations: A Mathematical Perspective*. World Scientific Publishing Company, Singapore, SINGAPORE, 2010.
- [41] Mustafa A Mohamad and Themistoklis P Sapsis. Probabilistic response and rare events in Mathieu’s equation under correlated parametric excitation. *Ocean Engineering*, 120:289–297, 2016.
- [42] Krikamol Muandet, Kenji Fukumizu, Bharath Sriperumbudur, and Bernhard Schölkopf. Kernel Mean Embedding of Distributions: A Review and Beyond. *Foundations and Trends® in Machine Learning*, 10(1-2):1–141, 2017.
- [43] Radford M. Neal. Annealed importance sampling. *Statistics and Computing*, 11(2):125–139, April 2001.
- [44] Frank Noé, Simon Olsson, Jonas Köhler, and Hao Wu. Boltzmann generators: Sampling equilibrium states of many-body systems with deep learning. *Science*, 365(6457), September 2019.

- [45] Matthew D Parno and Youssef M Marzouk. Transport map accelerated Markov Chain Monte Carlo. *SIAM/ASA Journal on Uncertainty Quantification*, 6(2):645–682, 2018.
- [46] Grigorios A. Pavliotis. *Stochastic Processes and Applications: Diffusion Processes, the Fokker-Planck and Langevin Equations*. Texts in Applied Mathematics. Springer-Verlag New York, 2014.
- [47] Maziar Raissi, Paris Perdikaris, and George E Karniadakis. Physics-informed neural networks: A deep learning framework for solving forward and inverse problems involving nonlinear partial differential equations. *Journal of Computational physics*, 378:686–707, 2019.
- [48] Sebastian Reich and Colin Cotter. *Probabilistic forecasting and Bayesian data assimilation*. Cambridge University Press, 2015.
- [49] Danilo Rezende and Shakir Mohamed. Variational inference with normalizing flows. In *International conference on machine learning*, pages 1530–1538. PMLR, 2015.
- [50] Lars Ruthotto and Eldad Haber. An introduction to deep generative modeling. *GAMM-Mitteilungen*, 44(2):e202100008, 2021.
- [51] Ruoqi Shen and Yin Tat Lee. The Randomized Midpoint Method for Log-Concave Sampling. In H. Wallach, H. Larochelle, A. Beygelzimer, F. d'Alché-Buc, E. Fox, and R. Garnett, editors, *Advances in Neural Information Processing Systems*, volume 32. Curran Associates, Inc., 2019.
- [52] Yang Song, Jascha Sohl-Dickstein, Diederik P Kingma, Abhishek Kumar, Stefano Ermon, and Ben Poole. Score-Based Generative Modeling through Stochastic Differential Equations. In *International Conference on Learning Representations*, 2020.
- [53] Wenqing Sun, Jinqian Feng, Jin Su, and Yunyun Liang. Data driven adaptive Gaussian mixture model for solving Fokker–Planck equation. *Chaos: An Interdisciplinary Journal of Nonlinear Science*, 32(3), 2022.
- [54] Keju Tang, Xiaoliang Wan, and Qifeng Liao. Deep density estimation via invertible block-triangular mapping. *Theoretical and Applied Mechanics Letters*, 10(3):143–148, 2020.
- [55] Kejun Tang, Xiaoliang Wan, and Qifeng Liao. Adaptive deep density approximation for Fokker-Planck equations. *Journal of Computational Physics*, 457:111080, 2022.
- [56] Takeshi Teshima, Isao Ishikawa, Koichi Tojo, Kenta Oono, Masahiro Ikeda, and Masashi Sugiyama. Coupling-based Invertible Neural Networks Are Universal Diffeomorphism Approximators. In H. Larochelle, M. Ranzato, R. Hadsell, M.F. Balcan, and H. Lin, editors, *Advances in Neural Information Processing Systems*, volume 33, pages 3362–3373. Curran Associates, Inc., 2020.
- [57] Joseph F. Traub. Information-based complexity. In *Encyclopedia of Computer Science*, pages 850–854. John Wiley and Sons Ltd., 2003.
- [58] Xiaoliang Wan and Shuangqing Wei. VAE-KRnet and Its Applications to Variational Bayes. *Communications in Computational Physics*, 31(4):1049–1082, 2022.
- [59] E Weinan, Jiequn Han, and Arnulf Jentzen. Algorithms for solving high dimensional PDEs: from nonlinear Monte Carlo to machine learning. *Nonlinearity*, 35(1):278, 2021.
- [60] Hassler Whitney. Analytic extensions of differentiable functions defined in closed sets. *Hassler Whitney Collected Papers*, pages 228–254, 1992.
- [61] René Wuttke, Hagen Hofmann, Daniel Nettels, Madeleine B Borgia, Jeetain Mittal, Robert B Best, and Benjamin Schuler. Temperature-dependent solvation modulates the dimensions of disordered proteins. *Proceedings of the National Academy of Sciences*, 111(14):5213–5218, 2014.
- [62] Yong Xu, Hao Zhang, Yongge Li, Kuang Zhou, Qi Liu, and Jürgen Kurths. Solving Fokker–Planck equation using deep learning. *Chaos: An Interdisciplinary Journal of Nonlinear Science*, 30(1), 2020.
- [63] Tang-Qing Yu, Jianfeng Lu, Cameron F. Abrams, and Eric Vanden-Eijnden. Multiscale implementation of infinite-swap replica exchange molecular dynamics. *Proc. Natl. Acad. Sci. U.S.A.*, 113(42):11744–11749, 2016.
- [64] Yaohua Zang, Gang Bao, Xiaojing Ye, and Haomin Zhou. Weak adversarial networks for high-dimensional partial differential equations. *Journal of Computational Physics*, 411:109409, 2020.
- [65] Jakob Zech and Youssef Marzouk. Sparse approximation of triangular transports, part II: The infinite-dimensional case. *Constructive Approximation*, 55(3):987–1036, 2022.
- [66] Li Zeng, Xiaoliang Wan, and Tao Zhou. Adaptive Deep Density Approximation for Fractional Fokker–Planck Equations. *Journal of Scientific Computing*, 97(3):68, 2023.
- [67] Jiayu Zhai, Matthew Dobson, and Yao Li. A deep learning method for solving Fokker–Planck equations. In *Mathematical and scientific machine learning*, pages 568–597. PMLR, 2022.
- [68] Benjamin J Zhang, Tuhin Sahai, and Youssef M Marzouk. A Koopman framework for rare event simulation in stochastic differential equations. *Journal of Computational Physics*, 456:111025, 2022.